

# Strong-coupling $d$ -wave superconductivity in $\text{PuCoGa}_5$ probed by point contact spectroscopy

D. Daghero,<sup>1</sup> M. Tortello,<sup>1</sup> G.A. Ummarino,<sup>1</sup> J.-C. Griveau,<sup>2</sup> E. Colineau,<sup>2</sup> R.  
Eloirdi,<sup>2</sup> A. B. Shick,<sup>2,3</sup> J. Kolorenc,<sup>3</sup> A. I. Lichtenstein,<sup>4</sup> and R. Caciuffo<sup>2</sup>

<sup>1</sup>*Dipartimento di Fisica, Politecnico di Torino,  
Corso Duca degli Abruzzi 24, 10129 Torino, Italy*

<sup>2</sup>*European Commission, Joint Research Centre,  
Institute for Transuranium Elements,  
Postfach 2340, D-76125 Karlsruhe, Germany*

<sup>3</sup>*Institute of Physics, ASCR, Na Slovance 2, CZ-18221 Prague, Czech Republic*

<sup>4</sup>*University of Hamburg, Jungiusstrasse 9, 20355 Hamburg, Germany*

(Dated: November 8, 2018)

PACS numbers: 74.70.Tx, 74.45.+c, 74.20.Mn, 74.20.Pq

A century on from its discovery, a complete fundamental understanding of superconductivity is still missing. Considerable research efforts are currently devoted to elucidating mechanisms by which pairs of electrons can bind together through the mediation of a boson field different than the one associated to the vibrations of a crystal lattice. PuCoGa<sub>5</sub>, a 5*f*-electron heavy-fermion superconductor with a record critical temperature  $T_c = 18.5$  K, is one of the many compounds for which the short-range, isotropic attraction provided by simple electron-phonon coupling does not appear as an adequate glue for electron pairing. Magnetic, or virtual valence fluctuations may have an important role in the stabilization of the superconducting ground state in PuCoGa<sub>5</sub>, but the specific nature of the coupling mechanism remains obscure. Here, we report the results of point-contact spectroscopy measurements in single crystals of PuCoGa<sub>5</sub>. Andreev reflection structures are clearly observed in the low-temperature spectra, and unambiguously prove that the paired superconducting electrons have wavefunction with the *d*-wave symmetry of a four-leaf clover. A straightforward analysis of the spectra provide the amplitude of the gap and its temperature dependence,  $\Delta(T)$ . We obtain  $\Delta(T \rightarrow 0) = 5.1 \pm 0.3$  meV and a gap ratio,  $2\Delta/k_B T_c = 6.5 \pm 0.3$ , indicating that the compound is in the regime of strong electron-boson coupling. The gap value and its temperature dependence can be well reproduced within the Eliashberg theory for superconductivity if the spectral function of the mediating bosons has a spin-fluctuations-like shape, with a peak energy of 6.5 meV. Electronic structure calculations, combining the local density approximation with an exact diagonalization of the Anderson impurity model, provide a hint about the possible origin of the fluctuations.

PuCoGa<sub>5</sub>, discovered in 2002, has the highest critical temperature ( $T_c = 18.5$  K) among heavy-fermion superconductors [1]. Though the  $\alpha$ -activity and the toxicity of Pu make it unsuitable for practical purposes, this material has been challenging the researchers since its discovery. As a matter of fact, it seems to elude any classification. The Sommerfeld coefficient  $\gamma$ , as measured by specific-heat experiments, is between 58 and 95 mJ/(mol K) [1, 2]. The effective mass of electrons is about 1/5 of that measured for the isostructural unconventional superconductor CeCoIn<sub>5</sub>, [2], suggesting a smaller degree of electronic correlation.

The magnetic properties of PuCoGa<sub>5</sub> and their possible relationship with the superconducting pairing have been debated, mainly because of conflicting results about the magnitude

of the magnetic moment carried by the Pu ions. A Curie-Weiss susceptibility in the normal state was initially observed [1], as expected for fluctuating local  $\text{Pu}^{3+}$  moments. Successive  $\mu\text{SR}$  studies showed no static, normal-state electronic magnetism in  $\text{PuCoGa}_5$  [3, 4] and polarized neutron diffraction experiments showed a small and temperature-independent microscopic magnetization dominated by the orbital moment [27].

The amplitude of the gap (or at least of the gap ratio  $2\Delta/k_B T_c$ ) has been estimated by different techniques. Using nuclear magnetic resonance (NMR) to measure the Knight shift in the superconducting state of a sample with  $T_c=18.5$  K, Curro *et al.* obtain  $2\Delta/k_B T_c = 8$  ( $\Delta \sim 6.3$  meV) [11].

From the theoretical and computational point of view,  $\text{PuCoGa}_5$  is a real challenge. Various band structure calculations have been reported [8–13, 23, 29], showing that the details of the Fermi surface (FS) and the value of the local magnetic moment depend on the theoretical approach. In a local density/generalized gradient approximations (LDA/GGA), the FS is quasi-two dimensional [8, 11, 13, 23], with at least two nearly-cylindrical sheets, one hole-like around the  $\Gamma = (0, 0, 0)$  point of the reciprocal space  $(k_x, k_y, k_z)$ , and one electron-like around the  $M = (\pi, \pi, 0)$  point. This bears a similarity to what more recently observed in Fe-based superconductors. The coupling mechanism that seems to account for the high- $T_c$  superconductivity in iron pnictides (based on the nesting between hole and electron FS sheets through a vector associated with a peak in the spin susceptibility) had been proposed earlier for  $\text{PuCoGa}_5$  [10]. The FS remains qualitatively unchanged with the addition of the Coulomb- $U$  interaction [29].

Several experimental facts [2, 3, 11, 12, 15–17] suggest that in  $\text{PuCoGa}_5$  the electrons in the pairs have a mutual angular momentum  $\ell = 2$ , corresponding to a superconducting order parameter (OP) with  $d_{x^2-y^2}$  symmetry, *i. e.* the gap in the single-particle excitation spectrum has a line of nodes intersecting the Fermi surface. A direct proof of the gap symmetry is, however, still missing. This is an important point, as the symmetry of the OP is closely related to the pairing mechanism. For instance, whilst isotropic electron-phonon attraction favors the formation of zero-angular-momentum pairs, with a spherically symmetric OP,  $d$ -wave symmetry is most easily realized if the pairing interaction is repulsive at short-range and anisotropic at larger distances, as the one provided by effective spin-spin couplings on the border of antiferromagnetism [19].

A magnetic nature of the Cooper pairing mediator in  $\text{PuCoGa}_5$  has been discussed by several

authors (see Ref. [20] for a recent review). Flint et al. [21] considered virtual valence fluctuations of the magnetic Pu configurations, creating Kondo screening channels with different symmetry, and demonstrated that in a lattice of magnetic ions, exchanging spin with conduction electrons in two different channels, a condensate of composite pairs between local moments and electrons is formed. These models must be reconciled with the temperature-independent susceptibility observed in the normal state [27]. A phononic mechanism in the framework of the  $d$ -wave Eliashberg theory has been discussed in Ref. [12]. Although able to reproduce a number of experimental observations, this model requires an electron-phonon ( $e$ - $ph$ ) coupling constant  $\lambda$  that is much higher than the value experimentally deduced from the time relaxation of photo-induced quasiparticles [22] ( $\lambda = 0.2$ - $0.26$ ).

We performed point-contact Andreev-reflection spectroscopy (PCARS) measurements in freshly annealed single crystals of  $^{239}\text{PuCoGa}_5$ , grown by a flux method and characterized by x-ray diffraction, electrical resistivity, magnetization and specific heat measurements. The point contacts were made between a fresh, mirror-like surface of the crystal (just exposed by breaking the sample) and a thin Au wire (about  $10\ \mu\text{m}$  in diameter). The uneven broken surface on which the contact is made prevents a fine control of the direction of current injection with respect to the crystallographic axes. However, as shown below, this does not prevent the unambiguous determination of the amplitude and symmetry of the OP.

Fig. 1 presents the temperature dependence of the raw conductance curves of a point contact whose normal-state resistance is  $6.2\ \Omega$ . All the curves but the lowest-temperature one are shifted downward for clarity. The top curve is measured at  $T = 1.8\ \text{K}$ , that means about  $T_c/10$ . This ensures that the gap extracted from it is well representative of the gap for  $T \rightarrow 0$ . The high-energy tails of the conductance curves are temperature independent, as shown in the inset, where the curves measured at  $T = 1.8\ \text{K}$  and in the normal state are reported without vertical offset as an example. This demonstrates that the contact is in the perfectly ballistic regime, with no contribution from Maxwell terms in the contact resistance, i.e. there is no diffusion in the contact region and the maximum excess energy with which the electrons are injected into the superconductor is exactly  $eV$ . Meeting this condition is essential for energy-resolved spectroscopy to be possible. The absence of heating effects in the contact is also witnessed by the coincidence between the *Andreev critical temperature*  $T_c^A$  (i.e. the temperature at which the Andreev signal disappears and the normal-state conductance is recovered, here between  $18.0\ \text{K}$  and  $18.5\ \text{K}$ ) and the bulk  $T_c$ , as determined from resistivity measurements ( $T_c = 18.1\ \text{K}$ , see

Fig. 6 in the Supplementary Material).

It is worth noticing that the point-contact curves in PuCoGa<sub>5</sub> do not show the strong asymmetry observed for CeCoIn<sub>5</sub> below the temperature where a coherent heavy-fermion liquid develops [35]. The asymmetric conductance in CeCoIn<sub>5</sub> has been explained in terms of a Fano resonance involving localized states near the interface and itinerant heavy electrons in the bulk [36]. The absence of a strong, temperature dependent asymmetry in PuCoGa<sub>5</sub> may thus confirm that superconductivity develops out of an incoherent metallic state [25].

In order to compare the experimental curves to the theoretical ones, a normalization is required, i.e. a division by the conductance of the same point contact when the superconductor is in the normal state. Because of the extremely high value of the upper critical field in PuCoGa<sub>5</sub>, this cannot be achieved by applying a magnetic field to suppress superconductivity at low temperature. However, owing to the moderate  $T_c$  and the negligible temperature dependence of the normal state conductance (witnessed by the absence of any change in shape of the tails of the conductance curves at  $|eV| > 15$  meV) we can safely normalize the conductance curves at any  $T < T_c^A$  by the normal state conductance curve measured at (or just above)  $T_c^A$ .

The result of this normalization is shown in Fig. 2 for two contacts made on different places of freshly-broken surfaces of the same sample. The two contacts have the same  $T_c^A$  but different normal-state resistance  $R_N$ . The curve shown in Fig. 2a presents a very clear zero-bias conductance peak (ZBCP), whose amplitude (greater than 2) can only be explained by assuming a nodal OP with a change of sign at the Fermi surface. Indeed, the shape of the conductance curve is similar to those shown for a dimensionless barrier strength  $Z = 1$  [1, 2] in Fig. (1d) of the Supplementary Material, and clearly indicates that the OP has a  $d$ -wave symmetry. The peak is ascribed to zero-energy Andreev bound states, arising from the constructive interference between electron-like and hole-like quasiparticles that feel order parameters with different signs [3].

Another important point to notice is that, unlike in other heavy-fermion compounds like CeCoIn<sub>5</sub> [36], the Andreev signal is very high in the superconducting phase; the curve is similar to the best ones ever observed in cuprates [29–32]. It thus seems that in PuCoGa<sub>5</sub> there is no need to assume multichannel tunneling in the presence of localized states near the interface, as instead is the case in CeCoIn<sub>5</sub> [36].

The conductance curve shown in Fig. 2b has a very different shape than the curve in Fig. 2a, reflecting a change from  $\alpha = \pi/4$  to  $\alpha = \pi/8$  of the angle between the direction of the

current injection (here in the  $k_x$ - $k_y$  plane) and the  $k_x$  axis. As a matter of fact, the curve in Fig. 2b looks similar to those shown in Fig. (1c) of the Supplementary Material, which have been obtained at  $T = 0$  for intermediate values of  $Z$  (0.5-0.7) and a misorientation angle  $\alpha = \pi/8$ .

Solid lines in Fig. 2 are the results of a quantitative spectral analysis using the 2-dimensional Blonder-Tinkham-Klapwijk (2D-BTK) formalism [1–3]. The parameters of the model are  $\Delta$  (here intended as the maximum amplitude of the gap), the barrier strength  $Z$ , the angle  $\alpha$ , and a broadening parameter  $\Gamma$  that must usually be included in the model when fitting experimental curves. Here  $\Gamma \ll \Delta$  so that it does not add any ambiguity to the determination of the gap amplitude. The best-fitting values of these parameters are indicated in the labels. The fit of the curves gives very similar values of the gap, and this is certainly the most important result, but also the barrier and broadening parameters are very similar. This means that the very different shape of the two curves almost completely depends on the angle  $\alpha$  which is different in the two cases, as shown pictorially in the insets.

Fig. 3a shows an example of how the normalized conductance curves evolve on increasing temperature. The experimental data (symbols) are compared to the 2D-BTK fit (solid lines). The fit is rather good at any temperature; note that both  $Z$  and  $\alpha$  are independent on  $T$  and were thus kept constant for all curves. We also kept  $\Gamma$  nearly constant so that the only parameter that varies significantly with temperature is the gap amplitude  $\Delta$ .

The temperature dependence of the gap as obtained from the fit of three different sets of conductance curves (in three different contacts) is shown in Fig. 3b. It is clear that the values are rather well reproducible; at low temperature, the gap values range between 4.85 and 5.30 meV, corresponding to a gap ratio  $2\Delta/k_B T_c = 6.2 - 6.7$ . The vertical spread of gap values can be used to evaluate *a posteriori* the uncertainty on the gap itself; this is obviously much greater than the uncertainty arising from the fit of a single curve, which can be empirically determined as the range of gap values that allow an acceptable (i.e. within some confidence limit) fit of the conductance curve, when all the other parameters are varied as well. The spread of gap values is small at low temperature and maximum around 14 K. Although the general trend of the gap seems to be compatible with a BCS-like  $\Delta(T)$  dependence (but of course, with a non-BCS gap ratio), this uncertainty does not allow discussing it in detail.

The solid line in Fig. 3b is *not* a fit of the data, but is calculated within the strong-coupling theory for superconductivity (known as Eliashberg theory [4, 5]) by assuming that

the superconducting coupling is mediated by spin fluctuations. In particular, we used the typical spin-fluctuation spectrum with the form [8]:  $\alpha^2 F_d(\Omega) \propto \frac{\Omega \Omega_0 \vartheta(\Omega_{max} - \Omega)}{\Omega^2 + \Omega_0^2}$  where  $\Omega_0$  is the energy peak,  $\Omega_{max}$  is a cut off energy that we chose as being  $\Omega_{max} = 4\Omega_0$  [9]. The line in Fig. 3b is obtained by taking  $\Omega_0 = 6.5$  meV and using an electron-boson coupling constant  $\lambda = 2.37$ . Details of the calculations are given as Supplementary Material. Assuming physically reasonable values of the Coulomb pseudopotential  $\mu^*$  ( $0 \leq \mu^* \leq 0.2$ ) [5], the observed  $\Delta(T)$  curve pose a stringent limit on the characteristic boson energy, namely  $5.3 \leq \Omega_0 \leq 8$  meV. This energy range is compatible with that determined by recent NMR measurements [13] for the characteristic spin-fluctuation energy in PuCoGa<sub>5</sub>, that is  $4 \leq \Omega_S \leq 8$  meV.

As a test of the reliability and generality of the results discussed so far, we also performed PCARS measurements in <sup>242</sup>PuCoGa<sub>5</sub> crystals featuring a lower  $T_c = 14.5$  K, due to the presence of Sb impurities (less than 1 %). The experimental results (shown as Supplementary Material) have been analyzed following the procedure described above, using the *same* spectral function and coupling constant as in Fig. 3b. We obtain a gap ratio  $2\Delta/k_B T_c = 6.2 \pm 0.4$ , showing that  $\Delta(T \rightarrow 0)$  scales with  $T_c$ .

A scenario where magnetic fluctuations are responsible for the formation of the Cooper pairs in PuCoGa<sub>5</sub> must be reconciled with the observed temperature-independent magnetic susceptibility [27] that points to vanishing local moments at the Pu sites. A plausible explanation is provided by electronic structure calculations combining the local density approximation (LDA) with the exact diagonalization (ED) [38] of a discretized single-impurity Anderson model [16]. In this approach, the band structure obtained by the relativistic version of the full-potential linearized augmented plane wave method (FP-LAPW) [21] is consistently extended to account for the full structure of the *f*-orbital atomic multiplets and their hybridization with the conduction bands [19]. Details on this procedure are given in the Supplementary Material.

The resulting *f*-orbital density of states (DOS) is shown in Fig. 4a. Below the Fermi energy  $E_F$ , the DOS exhibits a three-peak structure that is typical for Pu and for a number of its compounds. Peaks characterized by the total moment  $j = 5/2$  occur at  $E_F$  (peak labelled A) and at about 1 eV below  $E_F$  (peak C). The  $j = 7/2$  peak B is located in between at approximately 0.5 eV below  $E_F$ . The DOS is in a reasonably good agreement with the results of the non-crossing approximation reported in Ref. [26].

Fig. 4b shows the valence histogram calculated by projecting the ground state of the impurity model  $|\Omega\rangle$  onto the Pu atomic eigenstates  $|m\rangle$  that correspond to an integer *f*-shell occupation

$n_m$ . The plotted probabilities  $P_m$  determine the  $f$ -orbital valence  $\langle n_f \rangle = \sum_m P_m n_m = 5.3$ . The highest obtained probability is  $P_5 = 0.63$ , followed by  $P_6 = 0.33$ . In addition, there are small but non-zero probabilities  $P_4 = 0.03$  and  $P_7 = 0.01$ . This result indicates a mixed-valence nature of the Pu  $f$  shell that consists of a mixture of a magnetic  $f^5$  sextet and a non-magnetic  $f^6$  singlet, which is similar to the case of  $\delta$ -Pu [43]. This mixed (also referred to as intermediate) valence is consistent with a large value of the  $\gamma$ -coefficient, as typically observed in the mixed-valence rare-earth-based materials. The same materials display a temperature-independent magnetic susceptibility at low temperatures if one of the involved atomic configurations is non-magnetic [44], which further strengthens the analogy between the mixed-valence rare-earth compounds and the  $f$ -electron physics in PuCoGa<sub>5</sub>.

The Pu  $f$  shell carries a non-vanishing average moment as it fluctuates between the singlet and the sextet. The expectation values  $\langle \hat{X}^2 \rangle = X(X + 1)$ , where  $X = S, L$  and  $J$ , calculated for the  $f$  shell give  $S^{(5f)} = 2.18$ ,  $L^{(5f)} = 4.05$  and  $J^{(5f)} = 2.43$  for the spin, orbital and total moments. In the same time, the ground state  $|\Omega\rangle$  of the entire impurity model is a singlet that corresponds to all angular momenta being equal zero ( $S = L = J = 0$ ). Therefore, the fluctuations in the  $f$  shell are accompanied by canceling antiferromagnetic fluctuations in the conduction bands, which can be viewed as a manifestation of the Kondo physics. In addition, our band-structure calculations suggest an antiferromagnetic instability due to the presence of a Fermi-surface sheet with a negative second derivative of the Drude plasma energy (Supplementary Material).

In conclusion, we have performed point-contact Andreev-reflection measurements in PuCoGa<sub>5</sub> single crystals with different values of  $T_c$  due to different degrees of disorder. We have shown that PCARS spectra unambiguously indicate that the OP has a  $d$ -wave symmetry, consistent with indirect indications from NMR and  $\mu$ SR measurements. The amplitude of the gap at  $T \rightarrow 0$  is  $\Delta = 5.1 \pm 0.3$ , as determined from the fit of different curves, and corresponds to a gap ratio  $2\Delta/k_B T_c = 6.4 \pm 0.4$ . In crystals with Sb impurities and a reduced  $T_c = 14.5$  K, the Andreev signal is greatly reduced, possibly because of a larger quasiparticle scattering in the superconducting bank arising from self-induced disorder and impurities. The gap scales with  $T_c$ , giving the same gap ratio as in the highest- $T_c$  crystals, within the experimental uncertainty. In both cases, the temperature dependence of the gap is consistent with the predictions of the Eliashberg theory for strong-coupling superconductivity if spin fluctuations provide the mediating bosons. A characteristic boson energy  $\Omega_0 = 6.5$  meV and a coupling constant  $\lambda = 2.37$



allow reproducing the low-temperature gap values. These results show that PuCoGa<sub>5</sub> is an unconventional, *d*-wave superconductor in the strong-coupling regime, and indicate spin fluctuations as the probable boson that mediates superconductivity. Such fluctuations would involve a time-dependent  $5f$  local moment dynamically compensated by a moment momentarily formed in the surrounding cloud of conduction electrons.

### **Acknowledgement**

This work has been performed at the Institute of Transuranium Elements within its Actinide User Laboratory program, with financial support to users provided by the European Commission.

### **Corresponding author**

Correspondence and requests for materials should be addressed to Roberto Caciuffo, roberto.caciuffo@ec.europa.eu, or to D. Daghero, dario.daghero@polito.it.

### **Author contributions**

R.C., D.D, and M. T. designed research; D.D., M.T., and J.-C.G. performed PCARS experiments; R.E., J.-C.G., and E.C. prepared and characterized the samples; G.A.U. performed Eliashberg calculations, A.B.S., J.K., and A.I.L. performed *ab initio* calculations, D.D., M.T., J.-C.G., E.C., R.C., G.A.U., A.B.S, and J.K. analyzed and interpreted data; R.C., D.D., M. T., A.B.S., and J.K. wrote the paper.

### **Competing financial interests**

The authors declare that they have no competing financial interests.

- 
- [1] Sarrao, J. L., Morales, L. A., Thompson, J. D., Scott, B. L., Stewart, G. R., Wastin, F., Rebizant, J., Boulet, P., Colineau, E., Lander, G. H., Plutonium-based superconductivity with a transition

- temperature above 18 K. *Nature* **420**, 297–299 (2002).
- [2] Bauer, E. D., Thompson, J. D., Sarrao, J. L., Morales, L. A., Wastin, F., Rebizant, J., Griveau, J.-C., Javorsky, P., Boulet, P., Colineau, E., Lander, G. H., Stewart, G. R., Structural Tuning of Unconventional Superconductivity in PuMGa<sub>5</sub> (M=Co,Rh). *Phys. Rev. Lett.* **93**, 147005 (2004).
- [3] Heffner, R. H., Bauer, E. D., Chung, B., Fluss, M. J., Higemoto, W., Ito, T. U., MacLaughlin, D. E., Morales, L. A., Morris, G. D., Ohishi, K., Sarrao, J. L., Shu, L.,  $\mu$ SR Studies of Pu Metal and the Pu-based Superconductor PuCoGa<sub>5</sub>. *J. Phys. Soc. Jpn.* **75S**, 14-19 (2006).
- [4] Morris, G. D., Heffner, R. H., Bauer, E. D., Morales, L. A., Sarrao, J. L., Fluss, M. J., MacLaughlin, D. E., Shu, L., Anderson, J. E.,  $\mu$ SR Studies of the superconducting order parameter in PuCoGa<sub>5</sub>. *Physica B* **374-375**, 180–183 (2006).
- [5] Hiess, A., Stunault, A., Colineau, E., Rebizant, J., Wastin, F., Caciuffo, R., Lander, G. H., Electronic State of PuCoGa<sub>5</sub> and NpCoGa<sub>5</sub> as Probed by Polarized Neutrons. *Phys. Rev. Lett.* **100**, 076403 (2008).
- [6] Curro, N. J., Caldwell, T., Bauer, E. D., Morales, L. A., Graf, M. J., Bang, Y., Balatsky, A. V., Thompson, J. D., Sarrao, J. L., Unconventional superconductivity in PuCoGa<sub>5</sub>. *Nature* **434**, 622–625 (2005).
- [7] Opahle, I., Oppeneer, P. M., Superconductivity Caused by the Pairing of Plutonium 5*f* Electrons in PuCoGa<sub>5</sub>. *Phys. Rev. Lett.* **90**, 157001 (2003).
- [8] Maehira, T., Hotta, T., Ueda, K., Hasegawa, A., Electronic Structure and the Fermi Surface of PuCoGa<sub>5</sub> and NpCoGa<sub>5</sub>. *Phys. Rev. Lett.* **90**, 207007 (2003).
- [9] Opahle, I., Elgazzar, S., Koepernik, K., Oppeneer, P. M., Electronic structure of the Pu-based superconductor PuCoGa<sub>5</sub> and of related actinide-115 compounds. *Phys. Rev. B* **70**, 104504 (2004).
- [10] Tanaka, K., Ikeda, H., Yamada, K., Theory of Superconductivity in PuCoGa<sub>5</sub>. *J. Phys. Soc. Jpn.* **73**, 1285-1289 (2004).
- [11] Shick, A. B., Janiš, V., Oppeneer, P. M., Effect of Coulomb Correlations on the Electronic Structure of PuCoGa<sub>5</sub>. *Phys. Rev. Lett.* **94**, 016401 (2005).
- [12] Pourovskii, L. V., Katsnelson, M. I., Lichtenstein, A. I., Correlation effects in electronic structure of PuCoGa<sub>5</sub>. *Phys. Rev. B* **73**, 060506 (2006).
- [13] Zhu, J.-X., Tobash, P. H., Bauer, E. D., Ronning, F., Scott, B. L., Haule, K., Kotliar, G., Albers, R. C., Wills, J. M., Electronic structure and correlation effects in PuCoIn<sub>5</sub> as compared

- to PuCoGa<sub>5</sub>. *unpublished*, arxiv:1106.4314 (2011).
- [14] Shick, A. B., Rusz, J., Kolorenč, J., Oppeneer, P. M., Havela, L., Theoretical investigation of electronic structure, electric field gradients, and photoemission of PuCoGa<sub>5</sub> and PuRhGa<sub>5</sub> superconductors. *Phys. Rev. B* **83**, 155105 (2011).
- [15] Bang, Y., Balatsky, A. V., Wastin, F., Thompson, J. D., Possible pairing mechanisms of PuCoGa<sub>5</sub> superconductor. *Phys. Rev. B* **70**, 104512 (2004).
- [16] Boulet, P., Colineau, E., Wastin, F., Rebizant, J., Javorský, P., Lander, G. H., Thompson, J. D., Tuning of the electronic properties in PuCoGa<sub>5</sub> by actinide (U, Np) and transition-metal (Fe, Rh, Ni) substitutions. *Phys. Rev. B* **72**, 104508 (2005).
- [17] Ohishi, K., Heffner, R. H., Morris, G. D., Bauer, E. D., Graf, M. J., Zhu, J.-X., Morales, L. A., Sarrao, J. L., Fluss, M. J., MacLaughlin, D. E., Shu, L., Higemoto, W., Ito, T. U., Muon spin rotation measurements of the superfluid density in fresh and aged superconducting PuCoGa<sub>5</sub>. *Phys. Rev. B* **76**, 064504 (2007).
- [18] Jutier, F., Ummarino, G. A., Griveau, J. -C., Wastin, F., Colineau, E., Rebizant, J., Magnani, N., Caciuffo, R., Possible mechanism of superconductivity in PuCoGa<sub>5</sub> probed by self-irradiation damage. *Phys. Rev. B* **77**, 024521 (2008).
- [19] Monthoux, P., Pines, D., Lonzarich, G. G., Superconductivity without phonons. *Nature* **450**, 1177-1183 (2007).
- [20] Pflüderer, C., Superconducting phases of *f*-electron compounds. *Rev. Mod. Phys.* **81**, 1551–1624 (2009).
- [21] Flint, R., Dzero, M., Coleman, P., Heavy electrons and the symplectic symmetry of spin. *Nature Physics* **4**, 643-648 (2008).
- [22] Talbayev, D., Burch, K. S., Chia, E. E. M., Trugman, S. A., Zhu, J.-X., Bauer, E. D., Kennison, J. A., Mitchell, J. N., Thompson, J. D., Sarrao, J. L., Taylor, A. J., Hybridization and Superconducting Gaps in the Heavy-Fermion Superconductor PuCoGa<sub>5</sub> Probed via the Dynamics of Photoinduced Quasiparticles. *Phys. Rev. Lett.* **104**, 227002 (2010).
- [23] Park, W. K., Sarrao, J. L., Thompson, J. D., Greene, L. H., Andreev Reflection in Heavy-Fermion Superconductors and Order Parameter Symmetry in CeCoIn<sub>5</sub>. *Phys. Rev. Lett.* **100**, 177001 (2008).
- [24] Fogelström, M., Park, W. K., Greene, L. H., Goll, G., Graf, M. J., Point-contact spectroscopy in heavy-fermion superconductors. *Phys. Rev. B* **82**, 014527 (2010).

- [25] Coleman, P., Handbook of Magnetism and Advanced Magnetic Materials. *ed. H. Kronmuller and S. Parkin. Vol 1: Fundamentals and Theory, John Wiley and Sons, 95-148 (2007).*
- [26] Blonder, G. E., Tinkham, M., Klapwijk, T. M., Transition from metallic to tunneling regimes in superconducting microconstrictions: Excess current, charge imbalance, and supercurrent conversion. *Phys. Rev. B* **25**, 4515–4532 (1982).
- [27] Kashiwaya, S., Tanaka, Y., Koyanagi, M., Kajimura, K., Theory for tunneling spectroscopy of anisotropic superconductors. *Phys. Rev. B* **53**, 2667–2676 (1996).
- [28] Daghero, D., Gonnelli, R. S., Probing multiband superconductivity by point-contact spectroscopy. *Supercond. Sci. Technol.* **23**, 043001 (2010).
- [29] Deutscher, G., Andreev–Saint-James reflections: A probe of cuprate superconductors. *Rev. Mod. Phys.* **77**, 109–135 (2005).
- [30] Wei, J. Y. T., Yeh, N.-C., Garrigus, D. F., Strasik, M., Directional Tunneling and Andreev Reflection on  $\text{YBa}_2\text{Cu}_3\text{O}_{7-\delta}$  Single Crystals: Predominance of  $d$ -Wave Pairing Symmetry Verified with the Generalized Blonder, Tinkham, and Klapwijk Theory. *Phys. Rev. Lett.* **81**, 2542–2545 (1998).
- [31] Biswas, A., Fournier, P., Qazilbash, M. M., Smolyaninova, V. N., Balci, H., Greene, R. L., Evidence of a  $d$ - to  $s$ -Wave Pairing Symmetry Transition in the Electron-Doped Cuprate Superconductor  $\text{Pr}_{2-x}\text{Ce}_x\text{CuO}_4$ . *Phys. Rev. Lett.* **88**, 207004 (2002).
- [32] Qazilbash, M. M., Biswas, A., Dagan, Y., Ott, R. A., Greene, R. L., Point-contact spectroscopy of the electron-doped cuprate superconductor  $\text{Pr}_{2-x}\text{Ce}_x\text{CuO}_4$ : The dependence of conductance-voltage spectra on cerium doping, barrier strength, and magnetic field. *Phys. Rev. B* **68**, 024502 (2003).
- [33] Eliashberg, G. M., Interactions between electrons and lattice vibrations in a superconductor. *Sov. Phys. JETP* **11**, 696–702 (1960).
- [34] Carbotte, J. P., Properties of boson-exchange superconductors. *Rev. Mod. Phys.* **62**, 1027–1157 (1990).
- [35] Millis, A. J., Monien, H., Pines, D., Phenomenological model of nuclear relaxation in the normal state of  $\text{YBa}_2\text{Cu}_3\text{O}_7$ . *Phys. Rev. B* **42**, 167–178 (1990).
- [36] Monthoux, P., Balatsky, A. V., Pines, D., Toward a theory of high-temperature superconductivity in the antiferromagnetically correlated cuprate oxides. *Phys. Rev. Lett.* **67**, 3448–3451 (1991).
- [37] Baek, S. -H., Sakai, H., Bauer, E. D., Mitchell, J. N., and Kennison, J. A., Ronning, F., Thompson,

- J. D., Anisotropic Spin Fluctuations and Superconductivity in “115” Heavy Fermion Compounds:  $^{59}\text{Co}$  NMR Study in  $\text{PuCoGa}_5$ . *Phys. Rev. Lett.* **105**, 217002 (2010).
- [38] Kolorenč, J., *unpublished*.
- [39] Hewson, A. C., The Kondo Problem to Heavy Fermions. *Cambridge University Press* (1993).
- [40] Shick, A. B., Pickett, W. E., Magnetism, Spin-Orbit Coupling, and Superconducting Pairing in  $\text{UGe}_2$ . *Phys. Rev. Lett.* **86**, 300–303 (2001).
- [41] Shick, A. B., Kolorenč, J., Lichtenstein, A. I., Havela, L., Electronic structure and spectral properties of Am, Cm, and Bk: Charge-density self-consistent LDA+HIA calculations in the FP-LAPW basis. *Phys. Rev. B* **80**, 085106 (2009).
- [42] Pezzoli, M. E., Haule, K., Kotliar, G., Neutron Magnetic Form Factor in Strongly Correlated Materials. *Phys. Rev. Lett.* **106**, 016403 (2011).
- [43] Shim, J. H., Haule, K., Kotliar, G., Fluctuating valence in a correlated solid and the anomalous properties of  $\delta$ -plutonium. *Nature* **446**, 513–516 (2007).
- [44] Lawrence, J. M., Riseborough, P. S., Parks, R. D., Valence fluctuation phenomena. *Rep. Prog. Phys.* **44**, 1–84 (1981).

# Supplementary material for "Strong-coupling $d$ -wave superconductivity in PuCoGa<sub>5</sub> probed by point contact spectroscopy"

## I. POINT CONTACT ANDREEV REFLECTION SPECTROSCOPY

Point contact spectroscopy is a simple but very powerful tool for the investigation of the superconducting order parameter (OP) that, in the past decades, has been successfully applied, among others, to cuprates, borocarbides, multiband superconductors and even to the recently discovered iron-based superconductors. The technique consists in creating a N-S contact between a normal metal (N) and a superconductor (S), whose radius  $a$  is smaller than both the electronic mean-free path and the coherence length in S. In these conditions, an electron travels through the contact ballistically, i.e. without being diffused, so that if a voltage  $V$  is kept at the junction's end, it enters the superconductor with a maximum excess energy  $eV$ . When this energy is smaller than the gap in the superconductor,  $\Delta$ , the electron cannot propagate in S as an electron-like quasiparticle (ELQ), because it finds no available states. Thus, it forms a Cooper pair and a hole is retro-reflected in N.

If the gap is isotropic (Fig. 5a, top) and there is no potential barrier at the interface, this results in a doubling of the conductance for  $|V| \leq \Delta/e$  (see Fig. 5b, top curve). If  $|eV| > \Delta$ , the conductance decreases again towards the value it would have if the superconductor was in the normal state. If a barrier is present, other phenomena take place that can give rise to a normal reflection of the incoming electron, and also to the transmission of hole-like quasiparticles (HLQ) in S. As a result, the conductance presents two maxima at approximately  $V = \pm\Delta/e$  and a zero-bias minimum (see Fig. 5b).

If instead the energy gap has a dependence on the direction, i.e. the gap is anisotropic, electrons injected along different directions may experience different gap amplitudes. In this case, it is mandatory to integrate over all the possible directions along which the electrons can arrive to the interface. In particular, for a  $d_{x^2-y^2}$ -wave symmetry of the gap,  $\Delta(\theta, \phi) = \Delta_0 \cos(2\theta) \sin^2(\phi)$ , where  $\theta$  is the azimuthal angle in the  $k_x, k_y$  plane of the reciprocal space and  $\phi$  the inclination angle (see Fig. 5a, bottom), the shape of the conductance curves does not depend only on the height of the potential barrier at the interface, but also on the angle between the direction of current injection (i.e. the normal to the interface) and the  $k_x$  axis. This angle will be called  $\alpha$  in the following.

The curves shown in Fig. 5 were calculated by using the so called 2D-BTK model [1–3] where the problem is reduced to a two-dimensional one and the Fermi surface (FS) is supposed to be perfectly cylindrical (with its axis parallel to the  $k_z$  axis). This means that the dependence of the OP on  $\phi$  is disregarded. In this paper, based on the mostly 2D shape of the largest FS sheets and also for simplicity, we have always used this model. It can be shown [3] that, with respect to a more refined 3D model, this approximation generally gives rise to an overestimation of the parameter  $Z$ , proportional to the height of the potential barrier at the interface, which is not relevant in our analysis.

If  $\alpha = 0$ , for any angle of incidence ( $\theta$ ) of the incoming electron, ELQ and HLQ transmitted in S with angles  $+\theta$  and  $-\theta$  feel the same order parameter, in amplitude and sign. The conductance in this case is doubled only at zero bias where it shows a characteristic cusp. If there is no barrier, the same shape is obtained for any value of  $\alpha$ : the conductance curve always looks like the top curve in Fig. 5c. If instead a barrier is present, for any  $\alpha \neq 0$  some values of  $\theta$  exist for which HLQ and ELQ feel order parameters of opposite sign [3]. This gives rise to constructive interference between HLQ and ELQ that results in localized zero-energy states (Andreev bound states). These states manifest themselves in the conductance giving rise to a peak at zero bias (ZBCP). When  $\alpha = \pi/4$  the current is injected along the nodal direction, *all* ELQ and HLQ interfere and the ZBCP is maximum. An example of calculated (normalized) conductance curves assuming  $\alpha = \pi/8$  and  $\alpha = \pi/4$  is shown in Figs. 5c and 5d for increasing values of  $Z$ .

## II. SOLUTION OF ELIASHBERG EQUATIONS

In the imaginary-axis representation, the  $d$ -wave, one-band Eliashberg theory [4, 5] is formulated by the following equations for the gap  $\Delta_n(\phi) = \Delta(i\omega_n, \phi)$  and the renormalization functions  $Z_n(\phi) = Z(i\omega_n, \phi)$ :

$$\begin{aligned} \omega_n Z_n(\phi) &= \omega_n + \pi T \sum_m \int_0^{2\pi} \frac{d\phi'}{2\pi} \lambda_{nm}(\phi, \phi') N_m^Z(\phi') \\ &+ \gamma_d \frac{N_n^Z}{c^2 + (N_n^Z)^2}; \end{aligned} \quad (1)$$

$$\begin{aligned}
Z_n(\phi)\Delta_n(\phi) &= \pi T \sum_m \int_0^{2\pi} \frac{d\phi'}{2\pi} \\
&\times [\lambda_{nm}(\phi, \phi') - \mu^*(\phi, \phi')\vartheta(\omega_c - |\omega_m|)] N_m^\Delta(\phi'),
\end{aligned} \tag{2}$$

where  $\vartheta$  is the Heaviside function,  $\omega_c$  is a cut-off energy for the Coulomb pseudopotential  $\mu^*$ , and  $N_m^\Delta(\phi) = \Delta_m(\phi)/\sqrt{\omega_m^2 + \Delta_m^2(\phi)}$ ,  $N_m^Z(\phi) = \omega_m/\sqrt{\omega_m^2 + \Delta_m^2(\phi)}$ , and  $N_n^Z$  is an angular average of  $N_n^Z(\phi')$  over the Fermi surface.

The parameter  $\gamma_d$  is proportional to the concentration of defects and  $c$  is a parameter related to the electron phase shift for scattering off an impurity [6]. The  $n^{\text{th}}$  Matsubara frequency is defined as  $i\omega_n = i\pi T(2n - 1)$ , and  $T$  is the temperature;  $\lambda_{nm}(\phi, \phi') = \lambda(i\omega_m - i\omega_n, \phi, \phi')$  is related to the electron-boson spectral function  $\alpha^2(\Omega)F(\Omega, \phi, \phi')$  through the following equation:

$$\lambda(i\omega_m - i\omega_n, \phi, \phi') = \int_0^{+\infty} \frac{2\Omega\alpha^2 F(\Omega, \phi, \phi')}{(\omega_m - \omega_n)^2 + \Omega^2} d\Omega, \tag{3}$$

where  $\Omega$  is the boson frequency. We made the usual lowest-order approximation that both the electron-boson spectral function and the Coulomb pseudopotential contain separate  $s$ - and  $d$ -wave contributions [7]:

$$\alpha^2 F(\Omega, \phi, \phi') = \alpha^2 F_s(\Omega) + 2\alpha^2 F_d(\Omega)\cos(2\phi)\cos(2\phi') \tag{4}$$

and

$$\mu^*(\phi, \phi') = \mu_s^* + 2\mu_d^*(\Omega)\cos(2\phi)\cos(2\phi') \tag{5}$$

Then we assumed for simplicity that  $\alpha^2 F_s(\Omega) = \alpha^2 F_d(\Omega)$ , and that  $\alpha^2 F_d(\Omega)$  has the typical shape of spin fluctuation spectral functions [8]:  $\alpha^2 F_d(\Omega) \propto \frac{\Omega\Omega_0\vartheta(\Omega_{max}-\Omega)}{\Omega^2+\Omega_0^2}$  where  $\Omega_0$  is the energy peak,  $\Omega_{max}$  is a cut off energy  $\Omega_{max} = 4\Omega_0$  [9] and  $\omega_c = 3\Omega_{max}$ .

We then looked for solutions of the equations having pure  $d$ -wave symmetry for the gap function  $\Delta(\omega, \phi') = \Delta_d(\omega)\sqrt{2}\cos(2\phi')$  and pure  $s$ -wave form for the renormalization function  $Z(\omega, \phi') = Z_s(\omega)$ ; the reason for this choice is that the only solution of the homogeneous integral equation for  $Z_d(\omega)$  is  $Z_d(\omega) = 0$ , at least for reasonable values of  $\lambda_d$  [10]. Note that, if a  $d$ -wave symmetry for the gap function is assumed, the parameter  $\mu_s^*$  does not enter into the two relevant Eliashberg equations. Therefore, although it is certainly larger than  $\mu_d^*$ , it does not influence the solution. The free parameters are then:  $\gamma_d$ ,  $c$ ,  $\Omega_0$ ,  $\mu_d^*$  and  $\lambda = \int_0^{+\infty} \frac{2\Omega\alpha^2 F_d(\Omega)}{\Omega} d\Omega$ .



The parameters  $c$  and  $\gamma_d$  were estimated by reanalyzing the normalized local spin susceptibility from the NMR experiment by Curro et al. [11]; in particular, it was necessary to assume  $\gamma_d = 0.25$  meV and  $c = 0$  (unitary limit) to fit the shape of the curve [12]. The unitary limit is the only possible choice to reproduce the dependence of the critical temperature on disorder [12]. As for  $\mu_d^*$ , it generally ranges between 0 and 0.2 [5]. Finally, let us mention here that a range for  $\Omega_0$  was recently provided by NMR [13] measurements:  $4 \leq \Omega_0 \leq 8$  meV.

The value of  $\lambda$  was chosen so as to obtain the experimental critical temperature ( $T_c = 18.5$  K) by solution of the imaginary-axis Eliashberg equations, and then the experimental low-temperature gap  $\Delta$  by solution of the real-axis Eliashberg equations [14] for different values of  $\Omega_0$  and  $\mu_d^*$ . Fig. 6a shows the values of the gap as a function of  $\Omega_0$  for different values of  $\mu_d^*$ . The corresponding values of  $\lambda$  are shown in Fig. 6b. From the results of point-contact Andreev reflection measurement we know that, in PuCoGa<sub>5</sub> single crystals with  $T_c = 18.5$  K the low-temperature gap lies in the range 4.8-5.2 meV. As we can see from Fig. 6a, this corresponds to an interval of possible values of  $\Omega_0$  that goes from 5.3 to about 8.9. From the intersection of this range with that given by NMR measurement [13] one obtains  $5.3 \leq \Omega_0 \leq 8$  meV. Looking at Fig. 6b, it is clear that this corresponds to  $2.2 \leq \lambda \leq 3.7$ .

To reproduce the temperature dependence of the gap, we chose for simplicity  $\mu_d^* = 0$  and adjusted the values of  $\Omega_0$  and  $\lambda$ . We found that the experimental low-temperature gap and the  $T_c$  can be obtained with  $\Omega_0 = 6.5$  meV and  $\lambda = 2.37$ .

In order to obtain  $T_c = 14.5$  K it is necessary to increase the scattering parameter to  $\gamma_d = 1.6$  meV. In this way, we were able to reproduce the temperature dependence of the gap in the low- $T_c$  samples with the same values of  $\Omega_0$  and  $\lambda$  mentioned above (see Fig. 11c). This means that all the difference between the two sets of data can be ascribed to the greater amount of impurity scattering in the lower- $T_c$  crystals.

### III. ELECTRONIC STRUCTURE CALCULATIONS

Following Ref. [15] we consider the multi-band Hubbard Hamiltonian  $H = H^0 + H^{\text{int}}$ , where

$$H^0 = \sum_{i,j} \sum_{\gamma_1, \gamma_2} H_{i\gamma_1, j\gamma_2}^0 c_{i\gamma_1}^\dagger c_{j\gamma_2} = \sum_{\mathbf{k}} \sum_{\gamma_1, \gamma_2} H_{\gamma_1, \gamma_2}^0(\mathbf{k}) c_{\gamma_1}^\dagger(\mathbf{k}) c_{\gamma_2}(\mathbf{k}) \quad (6)$$

is the one-particle Hamiltonian found from *ab initio* electronic structure calculations of a periodic crystal. The indices  $i, j$  label lattice sites,  $\gamma = (lm\sigma)$  mark spinorbitals  $\{\phi_\gamma\}$ , and  $\mathbf{k}$  is a

vector from the first Brillouin zone. We assume that the electron-electron correlations between  $s$ ,  $p$ , and  $d$  electrons are well approximated within DFT, and consider the correlations between the  $f$  electrons introducing the interaction Hamiltonian

$$H^{\text{int}} = \frac{1}{2} \sum_i \sum_{m_1, m_2, m_3, m_4}^{\sigma, \sigma'} \langle m_1, m_2 | V_i^{ee} | m_3, m_4 \rangle c_{im_1\sigma}^\dagger c_{im_2\sigma'}^\dagger c_{im_4\sigma'} c_{im_3\sigma}. \quad (7)$$

The operator  $V^{ee}$  represents an effective on-site Coulomb interaction [15] expressed in terms of the Slater integrals  $F_k$  and the spherical harmonics  $|lm\rangle$ .

In what follows, the effects of the interaction Hamiltonian  $H^{\text{int}}$  on the electronic structure are modeled by a  $\mathbf{k}$ -independent one-particle selfenergy  $\Sigma(z)$ , which is constructed with the aid of an auxiliary impurity model describing the complete seven-orbital  $f$  shell including the full spherically symmetric Coulomb interaction, spin-orbit coupling (SOC), and crystal field (CF). The Hamiltonian of this multi-orbital impurity model can be written as [16]

$$\begin{aligned} H_{\text{imp}} = & \sum_{\substack{kmm' \\ \sigma\sigma'}} [\epsilon^k]_{mm'}^\sigma b_{km\sigma}^\dagger b_{km'\sigma'} + \sum_{m\sigma} \epsilon_f f_{m\sigma}^\dagger f_{m\sigma} \\ & + \sum_{mm'\sigma\sigma'} [\xi \mathbf{l} \cdot \mathbf{s} + \Delta_{\text{CF}}]_{mm'}^\sigma f_{m\sigma}^\dagger f_{m'\sigma'} \\ & + \sum_{\substack{kmm' \\ \sigma\sigma'}} \left( [V^k]_{mm'}^\sigma f_{m\sigma}^\dagger b_{km'\sigma'} + \text{h.c.} \right) \\ & + \frac{1}{2} \sum_{\substack{mm'm'' \\ m''\sigma\sigma'}} U_{mm'm''} f_{m\sigma}^\dagger f_{m'\sigma'}^\dagger f_{m''\sigma'} f_{m''\sigma}, \end{aligned} \quad (8)$$

where  $f_{m\sigma}^\dagger$  creates an electron in the  $f$  shell and  $b_{m\sigma}^\dagger$  creates an electron in the ‘‘bath’’ which consists of those host-band states that hybridize with the impurity  $f$  shell. The impurity-level position  $\epsilon_f$  and the bath energies  $\epsilon^k$  are measured from the chemical potential  $\mu$ . The parameters  $\xi$  and  $\Delta_{\text{CF}}$  specify the strength of the SOC and the size of the CF at the impurity. The parameter matrices  $V^k$  describe the hybridization between the  $f$  states and the bath orbitals at the energies  $\epsilon^k$ .

The band Lanczos method [17, 18] is employed to find the lowest-lying eigenstates of the many-body Hamiltonian  $H_{\text{imp}}$  and to calculate the one-particle Green’s function in the subspace of the  $f$  orbitals  $[G_{\text{imp}}(z)]_{mm'}^{\sigma\sigma'}$  at low temperature ( $k_{\text{B}}T = 1/500$  eV). The sought for selfenergy  $[\Sigma(z)]_{mm'}^{\sigma\sigma'}$  is then straightforwardly obtained from the inverse of the Green’s function matrix  $[G_{\text{imp}}(z)]_{mm'}^{\sigma\sigma'}$ . Note that for the Lanczos method to be applicable, the continuum of the bath

states is discretized. In particular, the calculations presented here utilize only a single value for the index  $k$ .

Once the selfenergy is known, the local Green's function  $G(z)$  for the electrons in the solid is calculated as

$$[G(z)]_{\gamma_1\gamma_2}^{-1} = [G_{\text{LDA}}(z)]_{\gamma_1\gamma_2}^{-1} - \Delta\epsilon \delta_{\gamma_1\gamma_2} - [\Sigma(z)]_{\gamma_1\gamma_2}, \quad (9)$$

where  $\Delta\epsilon$  accounts for the difference between the impurity and the lattice chemical potentials, and  $G_{\text{LDA}}(z)$  is the LDA Green's function,

$$[G_{\text{LDA}}(z)]_{\gamma_1\gamma_2} = \frac{1}{V_{\text{BZ}}} \int_{\text{BZ}} d^3k [z + \mu - H_{\text{LDA}}(\mathbf{k})]_{\gamma_1\gamma_2}^{-1}. \quad (10)$$

For the charge-density self-consistency, we employ the so-called local density matrix approximation (LDMA) [19]. In the LDMA, the occupation matrix

$$n_{\gamma_1\gamma_2} = -\frac{1}{\pi} \text{Im} \int_{-\infty}^{E_{\text{F}}} dz [G(z)]_{\gamma_1\gamma_2} \quad (11)$$

is self-consistently evaluated with the aid of the local Green's function  $G(z)$  from Eq. (9). The matrix  $n_{\gamma_1\gamma_2}$  is then used to construct an effective LDA+ $U$  potential  $V_U$  which is inserted into Kohn–Sham-like equations,

$$[-\nabla^2 + V_{\text{LDA}}(\mathbf{r}) + V_U + \xi(\mathbf{l} \cdot \mathbf{s})] \Phi_{\mathbf{k}}^b(\mathbf{r}) = \epsilon_{\mathbf{k}}^b \Phi_{\mathbf{k}}^b(\mathbf{r}). \quad (12)$$

These equations are iteratively solved until self-consistency over the charge density is reached. In each iteration, a new Green's function  $G_{\text{LDA}}(z)$  and a new value of the  $f$ -shell occupation are obtained from the solution of Eq. (12). Subsequently, a new selfenergy  $\Sigma(z)$  corresponding to the updated  $f$ -shell occupation is constructed. Finally, the next iteration is started by inserting the new  $G_{\text{LDA}}(z)$  and  $\Sigma(z)$  into Eq. (9). After the iterations are completed, the imaginary part of the local Green's function  $G(z)$  provides a means to estimate the valence-band photoemission (PE) spectra.

In the calculations we used the in-house implementation [20, 21] of the full-potential linearized augmented plane wave (FP-LAPW) method [22]. This FP-LAPW version includes all relativistic effects: scalar-relativistic and spin-orbit coupling. The calculations were carried out assuming a paramagnetic state with the LDA optimized [23] crystal structure parameters of PuCoGa<sub>5</sub>. The Slater integrals were chosen as  $F_0 = 4.0$  eV, and  $F_2 = 7.76$  eV,  $F_4 = 5.05$  eV, and  $F_6 = 3.07$  eV [24]. They corresponds to commonly accepted values for Coulomb  $U = 4.0$

eV and exchange  $J = 0.64$  eV. The SOC parameter was determined from LDA calculations as  $\xi = 0.28$  meV. The crystal-field effects were found to be negligible and we set  $\Delta_{\text{CF}} = 0$ .

The first and fourth terms in the impurity model, Eq. (8), are to a good approximation diagonal in the  $\{j, j_z\}$  representation, so that we only need to specify one bath state (six orbitals) with  $\epsilon_{k=1}^{j=5/2}$  and  $V_{k=1}^{j=5/2}$ , and another bath state (eight orbitals) with  $\epsilon_{k=1}^{j=7/2}$  and  $V_{k=1}^{j=7/2}$ . In order to determine these bath parameters, we assume that LDA represents the non-interacting model for PuCoGa<sub>5</sub>, that is, we associate the LDA solution with the Hamiltonian of Eq. (8) where we set the Coulomb interaction matrix  $U_{mm'm''m'''} = 0$ . The numerical values of the bath parameters are then found as follows: We calculate the LDA hybridization function  $\Delta = \frac{1}{\pi N_f} \text{Im Tr}[G_{\text{LDA}}^{-1}(\epsilon + i\delta)]$  for  $j = 5/2$  ( $N_f = 6$ ) and for  $j = 7/2$  ( $N_f = 8$ ), which is shown in Fig. 7. Assuming that the most important hybridization is the one occurring in the vicinity of  $E_F$ , we obtain  $V_{k=1}^{5/2,7/2}$  from the relation  $\sum_k |V_k^j|^2 \delta(\epsilon_k^j - \epsilon) = \Delta^j(\epsilon)$  [25] averaged over the energy interval  $\epsilon \in (E_F - 0.5 \text{ eV}, E_F + 0.5 \text{ eV})$ . The bath-state energies  $\epsilon_{k=1}^{5/2,7/2}$  are adjusted to approximately reproduce the LDA  $5f$ -states occupations  $n_f^{5/2}$  and  $n_f^{7/2}$ .

TABLE I:  $5f$ -states occupations  $n_f$ ,  $n_f^{5/2}$  and  $n_f^{7/2}$ ,  $\epsilon_1^{5/2,7/2}$  (eV),  $V_1^{5/2,7/2}$  (eV) for PuCoGa<sub>5</sub>.

$n_f$	$n_f^{5/2}$	$n_f^{7/2}$	$\epsilon_1^{5/2}$	$V_1^{5/2}$	$\epsilon_1^{7/2}$	$V_1^{7/2}$
5.14	4.38	0.76	0.25	0.29	-0.07	0.34

In what follows, we have adopted the fully-localized (or atomic-like) limit (FLL) for the double-counting term  $V_{dc} = U(n_f - 1/2) - J(n_f - 1)/2$  entering the definition of the LDA+ $U$  potential  $V_U$ . In the FP-LAPW calculations we set the radii of the atomic spheres to 3.1 a.u. (Pu), 2.3 a.u. (Co) and 2.3 a.u. (Ga). The parameter  $R \times K_{\text{max}} = 10.2$  determined the basis set size, and the Brillouin zone (BZ) sampling was performed with 1152  $k$  points. The self-consistent procedure defined by Eqs. (9)–(12) is repeated until the convergence of the  $f$ -manifold occupation  $n_f$  is better than 0.01.

The resulting  $f$ -orbital DOS (or, the one-particle spectral function) is shown in Fig. 4a of the main text. The DOS below  $E_F$  is in reasonably good agreement with Ref. [26]. Above  $E_F$ , the DOS obtained here differs somewhat from the DOS reported in Ref. [26] for a reason which is unclear at the moment. We estimate the electronic specific heat coefficient using the formula  $\gamma = \frac{\pi^2}{3} k_B^2 \text{Tr}[N(E_F)(1 - \frac{d\Sigma(\omega)}{d\omega})|_{\omega=0}]$  and we get  $\approx 40$  mJ K<sup>-2</sup> mol<sup>-1</sup> which is smaller than the experimentally estimated value of 80–100 mJ K<sup>-2</sup> mol<sup>-1</sup>. Note that a possible enhancement of

$\gamma$  due to the electron-phonon interaction is not taken into account.

Now we discuss the magnetic properties. The ground state of the cluster formed by the  $f$  shell and the bath, Eq. (8), is a singlet ( $S = L = J = 0$ ) that includes  $\langle n_f \rangle = 5.30$  in the  $f$  shell, and  $\langle n_{bath} \rangle = 8.70$  in the bath states. The spin  $S = 2.18$ , orbital  $L = 4.05$  and total  $J = 2.43$  moments are calculated for the  $f$  shell from the expectation values  $\langle \hat{X}^2 \rangle = X(X + 1)$ ,  $X = S, L, J$ . The individual components of the moments vanish,  $\langle \hat{S}_z \rangle = \langle \hat{L}_z \rangle = 0$ , unless the symmetry is broken by an external magnetic field. We carry out calculations with a small external magnetic field added to Eq. (8) in order to estimate the local  $f$ -shell susceptibility. These calculations yield  $\approx 0.3 \times 10^{-3} \mu_B/\text{T}$  which is somewhat smaller than the experimental value  $0.74 \times 10^{-3} \mu_B/\text{T}$  [27].

Qualitatively, the non-magnetic character of the composite electron cluster is linked to the mixed-valence nature of the Pu atom. The fluctuating local moment is compensated by corresponding dynamical fluctuations of the bath moment. The magnetic susceptibility  $\chi \sim \frac{1}{(T+T_{fc})}$  is anticipated, similar to a Kondo-singlet state, which remains constant for  $T \ll T_{fc}$ , as observed experimentally [27]. Note that neither the admixture of atomic-like  $f^5$  and  $f^6$  multiplets nor the Kondo-like screening of the  $f^5$  state localized moment [28] by the bath alone are sufficient to form a singlet ground state of the composite cluster formed by the  $f$ -shell and the bath. When the hybridization is set to zero in Eq. (8) (LDA+Hubbard-I approximation [29]) the resulting mixed-valence solution with  $\langle n_f \rangle = 5.3$  is not a singlet and the  $f$ -shell stays magnetic. On the other hand, when we force  $f^5$  solution in Eq. (8) and keep hybridization unchanged, the ground state of the composite electron cluster is not in a singlet either. In this sense, the admixture of the non-magnetic  $f^6$  to the magnetic  $f^5$  state enhances the dynamical screening of the local moment by the bath.

Comparison of theoretical and experimental PE spectra represents an important criterion of soundness of the electronic structure calculations. The use of the single-particle LDA DOS to compare with the PE spectrum is justified only in case of weak electron correlations among the  $5f$  states. For the  $5f$  states at the borderline between the localized and itinerant behavior neither the LDA nor the static-mean-field LDA+U theories are sufficient to accurately describe the PE since these approximations entirely miss the experimentally observed atomic-like multiplets. In Fig. 8 we show the total DOS for PuCoGa<sub>5</sub> as provided by our LDA+ED calculations. Overall, the agreement with the experimental PE data [30] is improved over LDA+Hubbard-I calculations reported earlier [29].

Now we discuss the static band-structure resulting from the solutions of Eq. (12). In fact, as it can be seen from Fig. 9 (upper panel), near  $E_F$  it is very similar to the static band structure obtained from LDA+HIA calculations [29]. The corresponding quasi-particle Fermi surfaces (FS) from Ref. [29] are shown in the lower panel of Fig. 9. There are four sheets (I–IV) composing the FS: sheets I and II are fairly three-dimensional and sheets III and IV are two-dimensional. Close similarities are revealed between these sheets and the Fermi surfaces from the previous LDA [23] and AMF-LDA+U calculations. As it was already noticed in Ref. [29], FS calculated with LDMA and LDA have very similar geometry.

Now we calculate the Drude plasma energy,  $\Omega_p = \sqrt{\frac{1}{3}\Omega_x^2 + \frac{1}{3}\Omega_y^2 + \frac{1}{3}\Omega_z^2}$  where the individual directional components  $\Omega_i$  are given by

$$\Omega_i^2 = \frac{e^2}{2\pi^2} \int_{\text{BZ}} d^3k v_i^2 \delta(E(\mathbf{k}) - E_F), \quad (13)$$

which leads to numerical value of  $\Omega_p = 3.8$  eV, as in previous LDA+HIA calculations [29]. Eventually, it leads to the same estimate for the electron-phonon coupling  $\lambda_{\text{tr}} \approx 2.5$  from the Bloch–Grüneisen transport theory.

In addition, we can estimate the type of the magnetic instability, ferro- or antiferromagnetic, for the band structure in Fig. 9. The paramagnetic susceptibility  $\chi_0(q, \omega)$  in the limit of small  $q$  and  $\omega$  can be expanded [31] as  $\chi_0(q, \omega) = N(E_F) - aq^2 + 1b\frac{\omega}{q}$ . In a simplified form [32], the coefficient  $a$  is proportional to a second derivative  $\frac{d^2\Omega_p^2(E)}{d^2E}|_{E=E_F}$  of the Drude plasma energy. The sign of this derivative indicates the type of magnetic instability. A positive sign corresponds to  $q = 0$  ferromagnetic fluctuations, whereas a negative sign to  $q \neq 0$  antiferromagnetic (or spin-spiral) fluctuations. In Table II we show the second derivative of  $\Omega_p(E)$  for all four FS bands calculated from cubic polynomial fits. Our estimate points to FS-II as a suitable candidate for  $q \neq 0$  antiferromagnetic instability. The electrons at FS-II, at least in principle, can be paired by anti-ferromagnetic fluctuations.

It is also to note that the shape of FS shown in the lower panel of Fig. 9 suggests a possibility of nesting between the hole-like FS-1 around the  $\Gamma = (0, 0, 0)$  point and electron-like FS-3 around the  $M = (\pi, \pi, 0)$  point. This large  $q \sim (\pi, \pi, 0)$  nesting-like feature can lead to a peak in the spin susceptibility, and promote the anti-ferromagnetic fluctuations to develop. This suggest similarities between the coupling mechanisms for the high- $T_c$  superconductivity in PuCoGa<sub>5</sub> and Fe-based superconductors [33].

TABLE II: The total DOS( $E_F$ ) in  $\text{eV}^{-1}$ , Drude plasma energy (eV), and its second derivative over energy at  $E_F$

	FS-I	FS-II	FS-III	FS-IV
DOS( $E_F$ ) (1/eV)	0.7	1.3	0.8	0.5
$\Omega_p(E_F)$ (eV)	1.1	2.7	1.9	1.5
$\frac{d^2\Omega_p^2(E_F)}{d^2E_F}$	49.71	-221.14	72.0	193.7

#### IV. CHARACTERIZATION OF THE INVESTIGATED SAMPLES

The samples used for these experiments have been characterized by magnetic susceptibility and electrical resistivity measurements, using commercial Quantum Design platforms (MPMS 7-T SQUID, and PPMS-9T).  $^{239}\text{PuCoGa}_5$  single crystals have been submitted to a thermal treatment to anneal the self-radiation damage. Fig. 10 shows the temperature dependence of the electrical resistivity measured for one of these crystals immediately after a thermal treatment. All the samples exhibited a critical temperature very close to the optimal value  $T_c = 18.5$  K. Point Contact Andreev Reflection Spectroscopy (PCARS) measurements were started within one day from the thermal treatment. PCARS measurements have also been performed on  $^{242}\text{PuCoGa}_5$  crystals featuring a lower  $T_c = 14.5$  K, due to the presence of Sb impurities (less than 1 %). The results obtained for these samples are presented in the following section.

#### V. PCARS MEASUREMENTS ON SAMPLES WITH $T_c = 14.5$ K

The point contacts were made on the side surface of the crystals so as to inject the current mainly along the  $ab$  planes. Unlike in the purest samples, here we used a small spot of Ag conducting paste between the Au wire and the sample to act as the N electrode and also to mechanically stabilize the contacts. Fig. 11a shows a series of conductance curves measured as a function of temperature in a contact with  $R_N = 6.9\Omega$ . The curves are vertically offset for clarity; as in the cases discussed for the sample with  $T_c = 18.5$  K, there is no shift of the tails on increasing temperature.

Fig. 11b reports the normalized low-temperature conductance of the same contact (top) and that of a different contact with a higher  $R_N = 18.8 \Omega$  (bottom). The experimental data (symbols) are compared against the relevant 2D-BTK fit (lines). It is worth noting that these

curves (and *all* the curves obtained in crystals with reduced  $T_c$ ) show a small Andreev signal, whose amplitude is similar to that observed in CeCoIn<sub>5</sub> [34, 35]. It seems however logical, in this case, to ascribe the small signal to the greater amount of disorder in the samples (and thus also on the surface) with respect to the purest crystals, rather than to intrinsic phenomena as proposed in [36]. The small amplitude and the consequent absence of very clear structures result in a greater uncertainty on the fitting parameters, since different sets of parameters can give equally good fits. Moreover, the fit requires a large  $\Gamma$  (although still smaller than  $\Delta$ ). As an alternative, and according to [36], one could assume that a fraction of the injected current tunnel into a non-superconducting band or set of states, and does not contribute to Andreev reflection. In the latter case, the values of  $\Gamma$  would be smaller but an additional parameter would be necessary.

Fig. 11c shows an example of temperature dependence of the gap extracted from the fit (symbols). The line is the curve calculated within the Eliashberg theory, by using the *same* spectral function and coupling constant as for the sample with  $T_c = 18.5$  K. The different  $T_c$  and the different gap amplitude arise only from the larger value of the quasiparticle scattering rate  $\gamma_d$  included in the Eliashberg equations to account for the disorder. Incidentally, while  $T_c = 18.5$  K is obtained by using  $\gamma_d = 0.25$  meV, the reduced  $T_c = 14.5$  K of this particular contact requires  $\gamma_d = 1.6$  meV. Note that also the gap ratio  $2\Delta/k_B T_c = 6.2 \pm 0.4$  is compatible with that obtained in the purest crystals.

- 
- [1] Blonder, G. E., Tinkham, M., Klapwijk, T. M., Transition from metallic to tunneling regimes in superconducting microconstrictions: Excess current, charge imbalance, and supercurrent conversion. *Phys. Rev. B* **25**, 4515–4532 (1982).
  - [2] Kashiwaya, S., Tanaka, Y., Koyanagi, M., Kajimura, K., Theory for tunneling spectroscopy of anisotropic superconductors. *Phys. Rev. B* **53**, 2667–2676 (1996).
  - [3] Daghero, D., Gonnelli, R. S., Probing multiband superconductivity by point-contact spectroscopy. *Supercond. Sci. Technol.* **23**, 043001 (2010).
  - [4] Eliashberg, G. M., Interactions between electrons and lattice vibrations in a superconductor. *Sov. Phys. JETP* **11**, 696–702 (1960).
  - [5] Carbotte, J. P., Properties of boson-exchange superconductors. *Rev. Mod. Phys.* **62**, 1027–1157



- (1990).
- [6] Carbotte, J. P., Jiang, C., Impurity effects on NMR and the Knight shift in a d-wave superconductor. *Phys. Rev. B* **49**, 6126–6131 (1994).
  - [7] Rieck, C. T., Fay, D., Tewordt, L., Energy gap,  $T_c$ , and density of states in high-temperature superconductors for retarded  $s$ - and  $d$ -wave interactions. *Phys. Rev. B* **41**, 7289–7292 (1990).
  - [8] Millis, A. J., Monien, H., Pines, D., Phenomenological model of nuclear relaxation in the normal state of  $\text{YBa}_2\text{Cu}_3\text{O}_7$ . *Phys. Rev. B* **42**, 167–178 (1990).
  - [9] Monthoux, P., Balatsky, A. V., Pines, D., Toward a theory of high-temperature superconductivity in the antiferromagnetically correlated cuprate oxides. *Phys. Rev. Lett.* **67**, 3448–3451 (1991).
  - [10] Musaelian, K. A., Betouras, J., Chubukov, A. V., Joynt, R., Mixed-symmetry superconductivity in two-dimensional Fermi liquids. *Phys. Rev. B* **53**, 3598–3603 (1996).
  - [11] Curro, N. J., Caldwell, T., Bauer, E. D., Morales, L. A., Graf, M. J., Bang, Y., Balatsky, A. V., Thompson, J. D., Sarrao, J. L., Unconventional superconductivity in  $\text{PuCoGa}_5$ . *Nature* **434**, 622–625 (2005).
  - [12] Jutier, F., Ummarino, G. A., Griveau, J. -C., Wastin, F., Colineau, E., Rebizant, J., Magnani, N., Caciuffo, R., Possible mechanism of superconductivity in  $\text{PuCoGa}_5$  probed by self-irradiation damage. *Phys. Rev. B* **77**, 024521 (2008).
  - [13] Baek, S. -H., Sakai, H., Bauer, E. D., Mitchell, J. N., and Kennison, J. A., Ronning, F., Thompson, J. D., Anisotropic Spin Fluctuations and Superconductivity in “115” Heavy Fermion Compounds: Co-59 NMR Study in  $\text{PuCoGa}_5$ . *Phys. Rev. Lett.* **105**, 217002 (2010).
  - [14] Ummarino, G. A., Caciuffo, R., Chudo, H., Kambe, S., Energy scale of the electron-boson spectral function and superconductivity in  $\text{NpPd}_5\text{Al}_2$ . *Phys. Rev. B* **82**, 104510 (2010).
  - [15] Lichtenstein, A. I., Katsnelson, M. I., Ab initio calculations of quasiparticle band structure in correlated systems: LDA++ approach. *Phys. Rev. B* **57**, 6884–6895 (1998).
  - [16] Hewson, A. C., The Kondo Problem to Heavy Fermions. *Cambridge University Press* (1993).
  - [17] Ruhe, A., Implementation aspects of band Lanczos algorithms for computation of eigenvalues of large sparse symmetric matrices. *Math. Comput.* **33**, 680-687 (1979).
  - [18] Meyer, H.-D., Pal, S., A band-Lanczos method for computing matrix elements of a resolvent. *J. Chem. Phys.* **91**, 6195-6204 (1989).
  - [19] Shick, A. B., Kolorenč, J., Lichtenstein, A. I., Havela, L., Electronic structure and spectral properties of Am, Cm, and Bk: Charge-density self-consistent  $LDA + HIA$  calculations in the

- FP-LAPW basis. *Phys. Rev. B* **80**, 085106 (2009).
- [20] Shick, A. B., Lichtenstein, A. I., Pickett, W. E., Implementation of the LDA+U method using the full-potential linearized augmented plane-wave basis. *Phys. Rev. B* **60**, 10763–10769 (1999).
- [21] Shick, A. B., Pickett, W. E., Magnetism, Spin-Orbit Coupling, and Superconducting Pairing in UGe<sub>2</sub>. *Phys. Rev. Lett.* **86**, 300–303 (2001).
- [22] Wimmer, E., Krakauer, H., Weinert, M., Freeman, A. J., Full-potential self-consistent linearized-augmented-plane-wave method for calculating the electronic structure of molecules and surfaces: O<sub>2</sub> molecule. *Phys. Rev. B* **24**, 864–875 (1981).
- [23] Opahle, I., Oppeneer, P. M., Superconductivity Caused by the Pairing of Plutonium 5*f* Electrons in PuCoGa<sub>5</sub>. *Phys. Rev. Lett.* **90**, 157001 (2003).
- [24] Moore, K. T., van der Laan, G., Nature of the 5*f* states in actinide metals. *Rev. Mod. Phys.* **81**, 235–298 (2009).
- [25] Gunnarsson, O., Andersen, O. K., Jepsen, O. and Zaanen, J., Jepsen, O., Zaanen, J., Density-functional calculation of the parameters in the Anderson model: Application to Mn in CdTe. *Phys. Rev. B* **39**, 1708–1722 (1989).
- [26] Pezzoli, M. E., Haule, K., Kotliar, G., Neutron Magnetic Form Factor in Strongly Correlated Materials. *Phys. Rev. Lett.* **106**, 016403 (2011).
- [27] Hiess, A., Stunault, A., Colineau, E., Rebizant, J., Wastin, F., Caciuffo, R., Lander, G. H., Electronic State of PuCoGa<sub>5</sub> and NpCoGa<sub>5</sub> as Probed by Polarized Neutrons. *Phys. Rev. Lett.* **100**, 076403 (2008).
- [28] Matsumoto, M. Yin, Q. Otsuki, J. Savrasov, S. Multiple quantum phase transitions of plutonium compounds, *Phys. Rev. B* **84**, 041105 (2011).
- [29] Shick, A. B., Rusz, J., Kolorenč, J., Oppeneer, P. M., Havela, L., Theoretical investigation of electronic structure, electric field gradients, and photoemission of PuCoGa<sub>5</sub> and PuRhGa<sub>5</sub> superconductors. *Phys. Rev. B* **83**, 155105 (2011).
- [30] Eloirdi, R., Havela, L., Gouder, T., Shick, A., Rebizant, J., Huber, F., Caciuffo, R., Photoelectron spectroscopy study of PuCoGa<sub>5</sub> thin films. *J. Nucl. Mater.* **385**, 8–10 (2009).
- [31] Larson, P., Mazin, I. I., Singh, D., Magnetism, critical fluctuations, and susceptibility renormalization in Pd. *Phys. Rev. B* **69**, 064429 (2004).
- [32] Jeong, T., Kyker, A., Pickett, W. E., Fermi velocity spectrum and incipient magnetism in TiBe<sub>2</sub>. *Phys. Rev. B* **73**, 115106 (2006).

- [33] Mazin, I.I., Singh, D., Johannes, M.D., Du, M.H., Unconventional superconductivity with a sign reversal in the order parameter of  $\text{LaFeAsO}_{1-x}\text{F}_x$ , *Phys. Rev. Lett.* **101**, 057003 (2008).
- [34] Park, W. K., Greene, L. H., Sarrao, J. L., Thompson, J. D., Andreev reflection at the normal-metal/heavy-fermion superconductor  $\text{CeCoIn}_5$  interface. *Phys. Rev. B* **72**, 052509 (2005).
- [35] Park, W. K., Sarrao, J. L., Thompson, J. D., Greene, L. H., Andreev Reflection in Heavy-Fermion Superconductors and Order Parameter Symmetry in  $\text{CeCoIn}_5$ . *Phys. Rev. Lett.* **100**, 177001 (2008).
- [36] Fogelström, M., Park, W. K., Greene, L. H., Goll, G., Graf, M. J., Point-contact spectroscopy in heavy-fermion superconductors. *Phys. Rev. B* **82**, 014527 (2010).

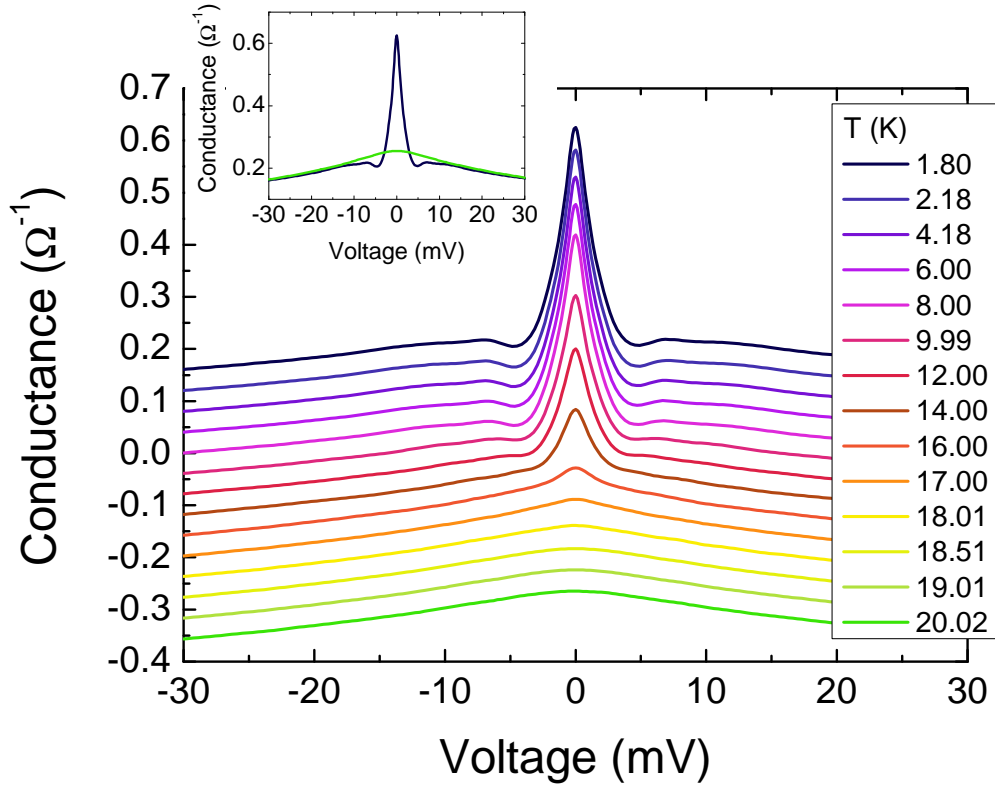


FIG. 1: Temperature dependence of the raw conductance curve of a Au/PuCoGa<sub>5</sub> point contact with  $R_N = 6.2\Omega$ . All the curves apart from the top one are vertically shifted for clarity. The inset shows the curve at 1.8 K and the curve at 20.02 K (and thus in the normal state) without any shift. The superposition of the tails is one of the indicators that the contact is in the ballistic regime.

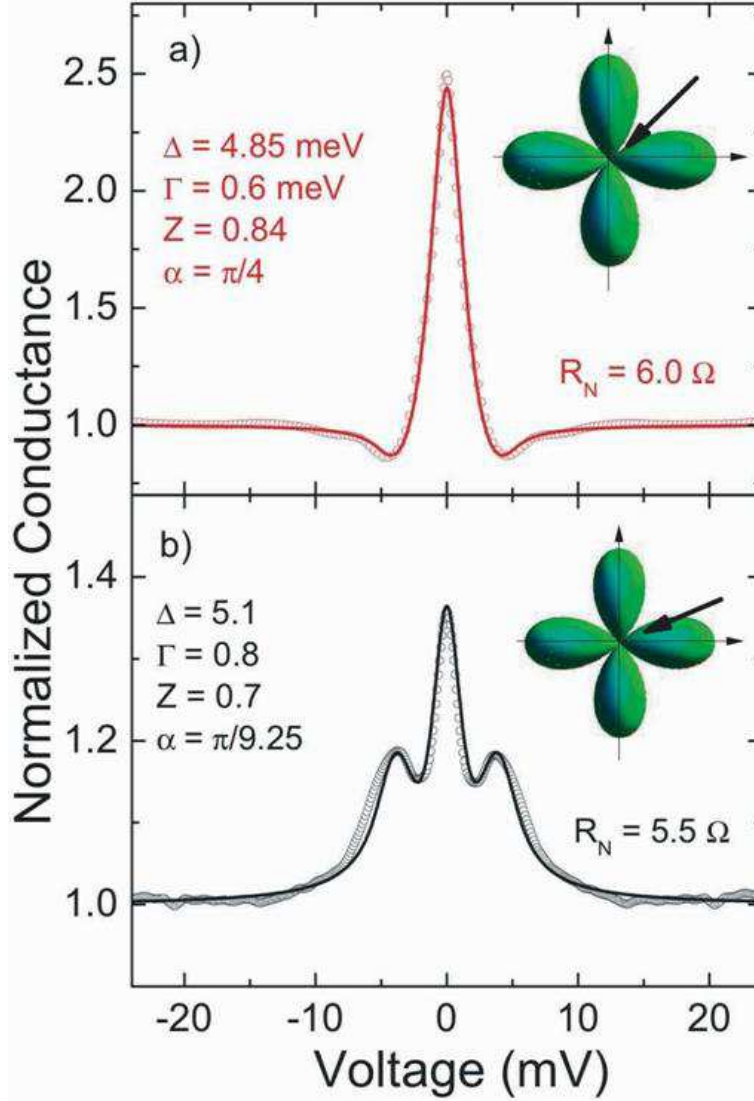


FIG. 2: Two examples of low-temperature conductance curves in  $\text{PuCoGa}_5$  after normalization (symbols) and the relevant 2D-BTK fit assuming a  $d$ -wave gap (lines). The values of the parameters are indicated in labels, as well as the normal-state resistance  $R_N$  of the corresponding Au/ $\text{PuCoGa}_5$  point contact.  $\Delta$  is the gap at  $T = 0$ ,  $\Gamma$  is a spectral broadening parameter,  $Z$  measures the barrier strength at the interface, and  $\alpha$  is the angle between the direction of current injection and the  $k_x$  axis. The different shape of the two curves simply arises from the different direction of the current injected with respect to the lobes of the  $d$ -wave symmetry (insets).

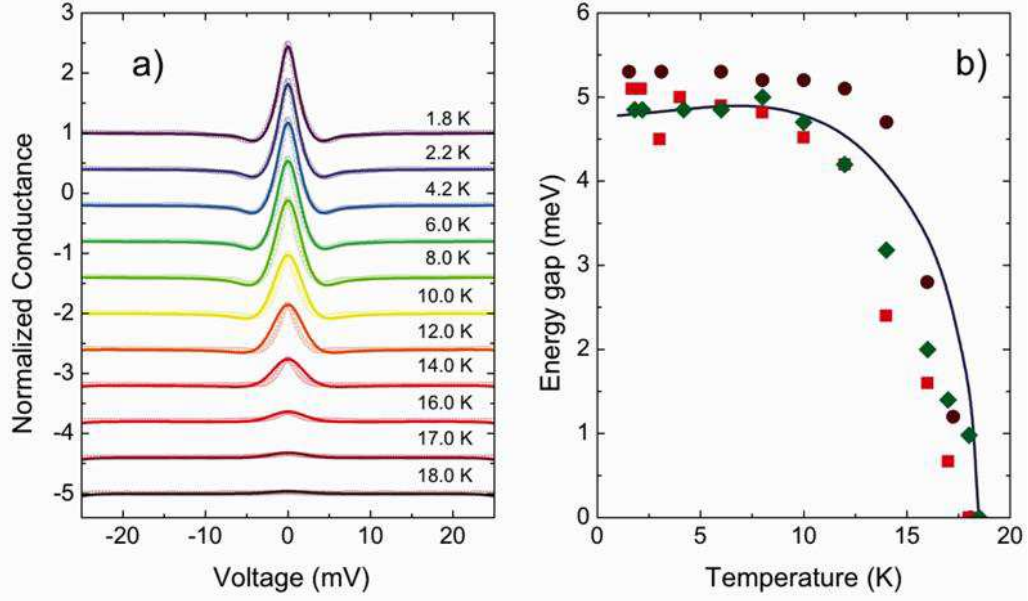


FIG. 3: (a) Temperature dependence of the normalized conductance curves of a contact with  $R_N = 6.0 \Omega$  (symbols) and their fit with the 2D-BTK model (lines). The curves are vertically offset for clarity. (b) Temperature dependence of the gap extracted from the fit of the conductance curves of three different contacts (symbols). The solid line is the  $\Delta(T)$  function calculated within the Eliashberg theory by assuming a spin-fluctuation spectrum peaked at  $\Omega_0 = 6.5$  meV and a coupling constant  $\lambda = 2.37$ .

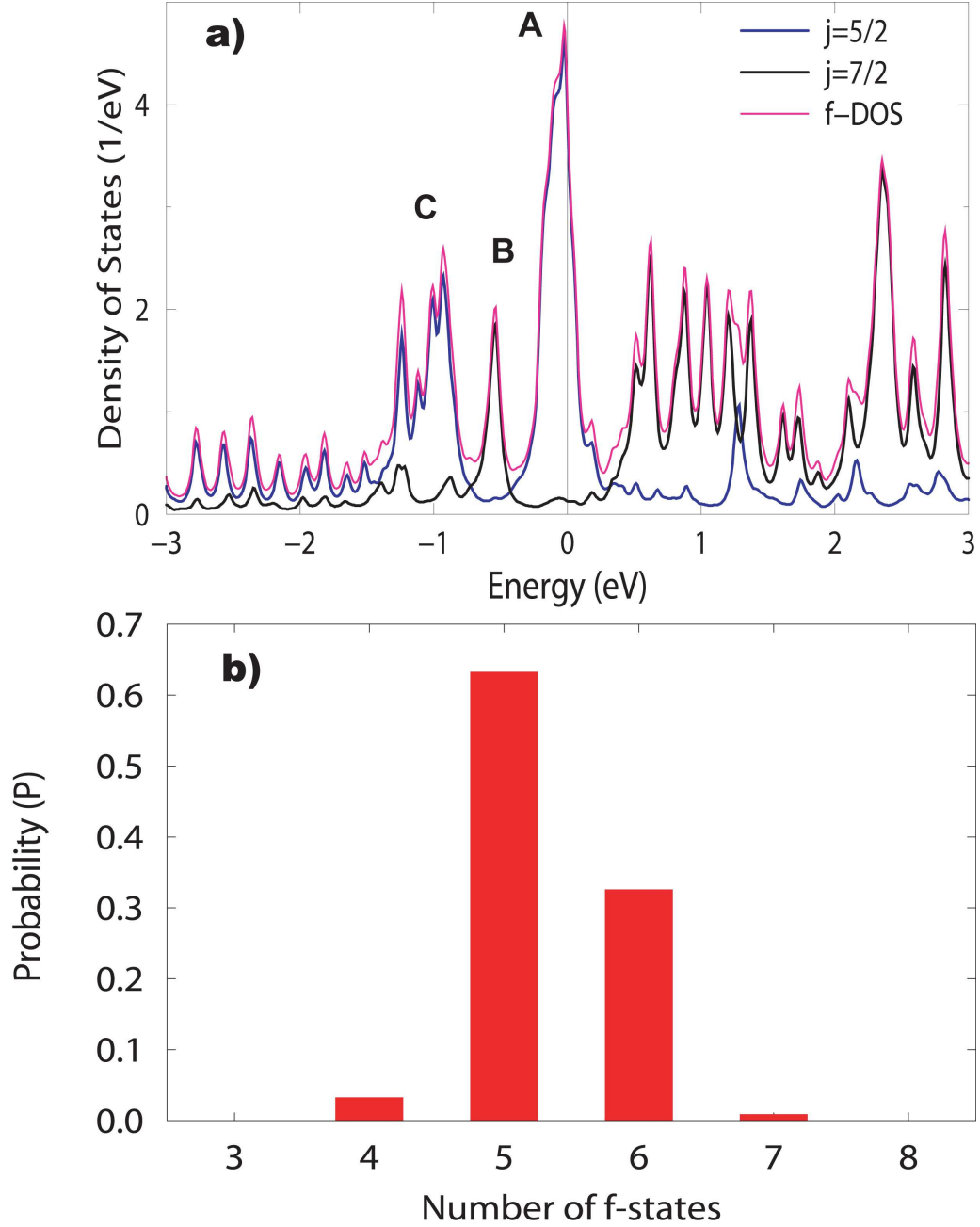


FIG. 4: (a)  $f$ -electron density of states (DOS) for the Pu atom in PuCoGa<sub>5</sub>:  $j = 5/2, 7/2$  projected, and total; (b) Valence histogram obtained by the projection of the LDA+ED solution onto Pu atomic eigenfunctions.

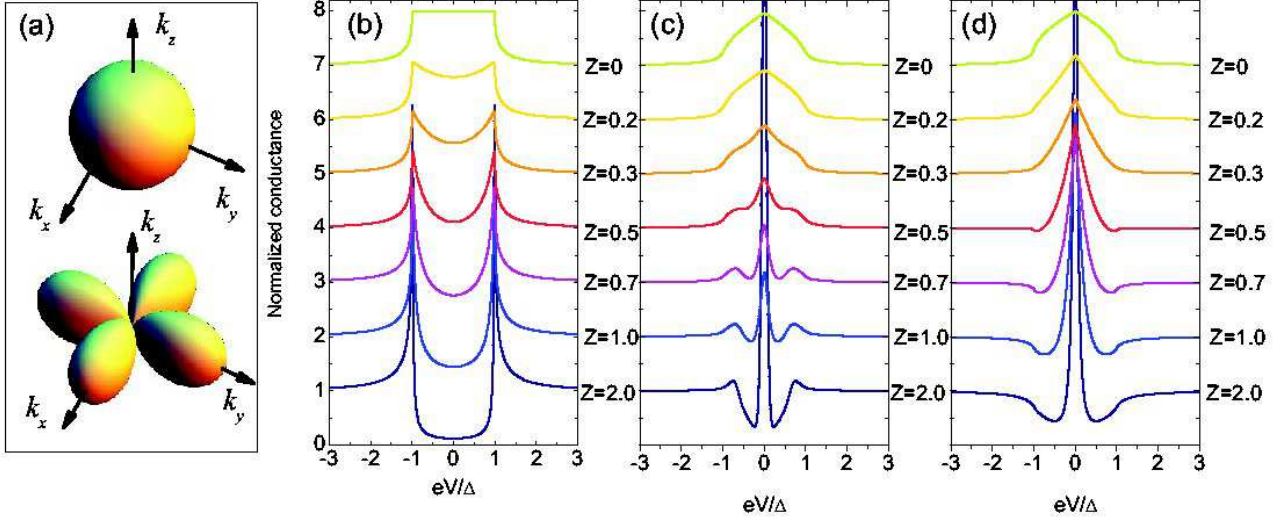


FIG. 5: (a) Amplitude of the order parameter in spherical coordinates in the reciprocal space. The cases of a  $s$ -wave (top) and of a  $d$ -wave (bottom) order parameter are shown. (b): Theoretical normalized conductance curves calculated at  $T = 0$  for a  $s$ -wave gap, and different values of the dimensionless barrier strength  $Z$ . (c,d) Normalized conductance curves at  $T=0$  calculated with the 2D-BTK model for a  $d$ -wave gap and assuming  $\alpha = \pi/8$  and  $\alpha = \pi/4$ , respectively;  $\alpha$  is the angle between the direction of the injected current and the  $k_x$  axis.



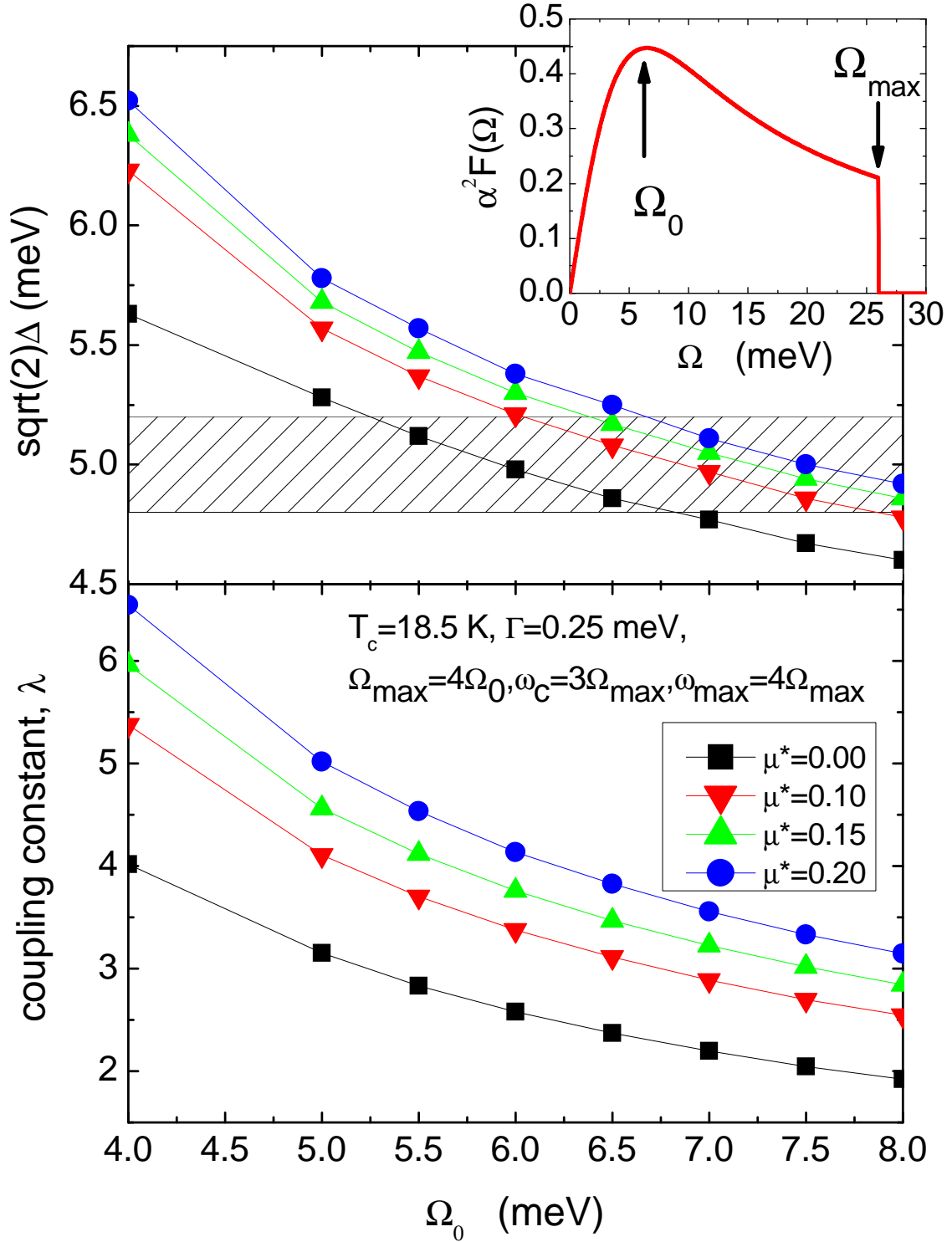


FIG. 6: (a) The effect of  $\Omega_0$  on  $\Delta$  for different values of the Coulomb pseudopotential  $\mu_d^*$ . The dashed region indicates the range of gap values extracted from the point contact Andreev reflection measurements. The inset shows the shape of the electron-spin-fluctuation spectrum. (b) The effect of  $\Omega_0$  on the coupling constant  $\lambda$  for different values of the Coulomb pseudopotential.

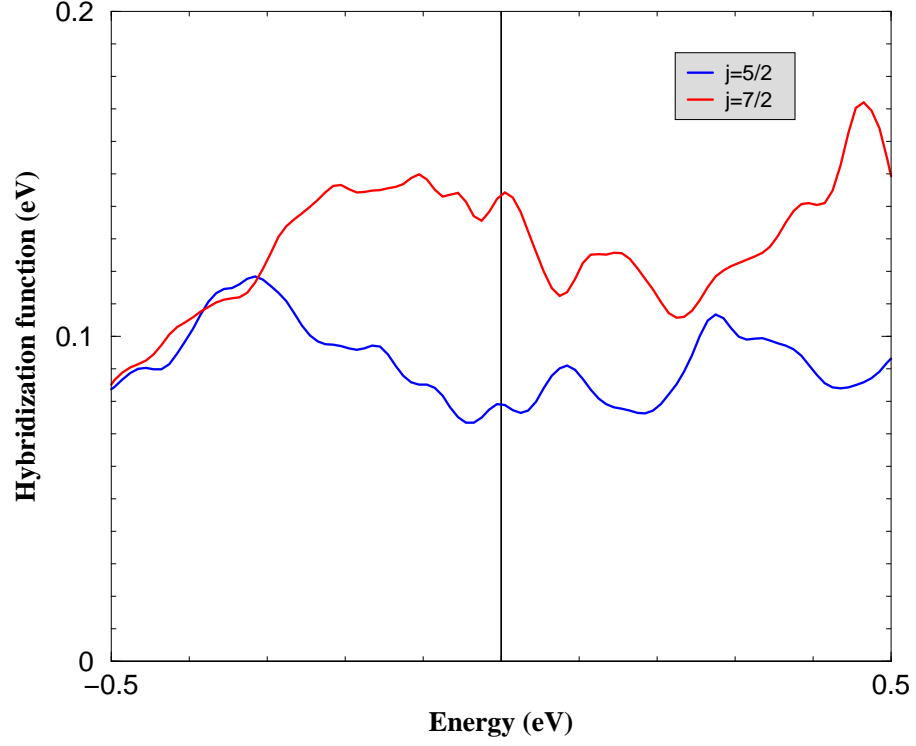


FIG. 7: (Color online) LDA hybridization function  $\Delta = \frac{1}{\pi N_f} \text{ImTr}[G^{-1}(\epsilon + i\delta)]$  for  $j = 5/2$  and  $7/2$  and  $\delta = 31.4$  meV.

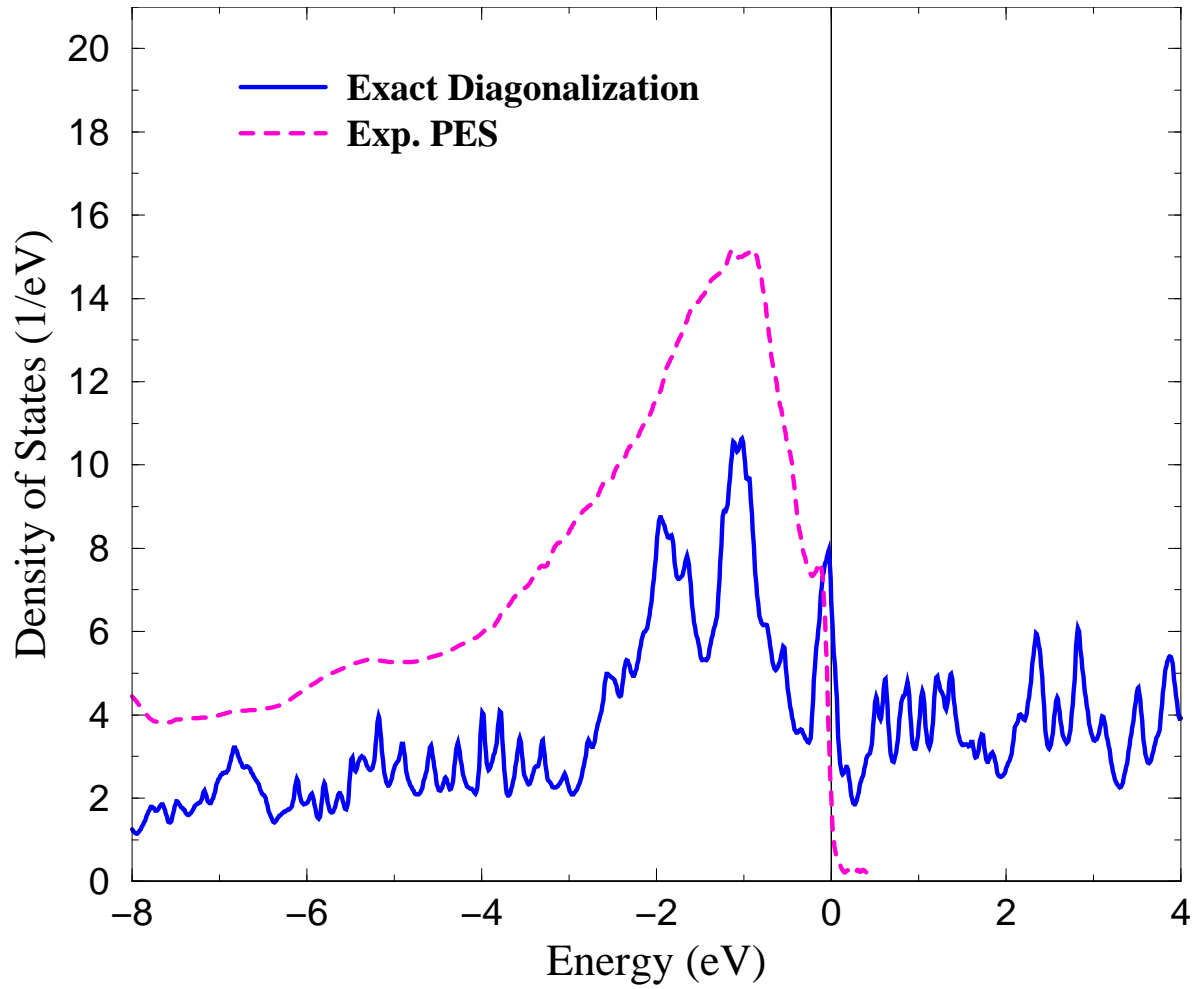


FIG. 8: (Color online) Total DOS of PuCoGa<sub>5</sub> provided by LDA+ED with  $U = 4.0$  eV. The experimental PE spectrum (arb. units) is taken from Ref. [30].

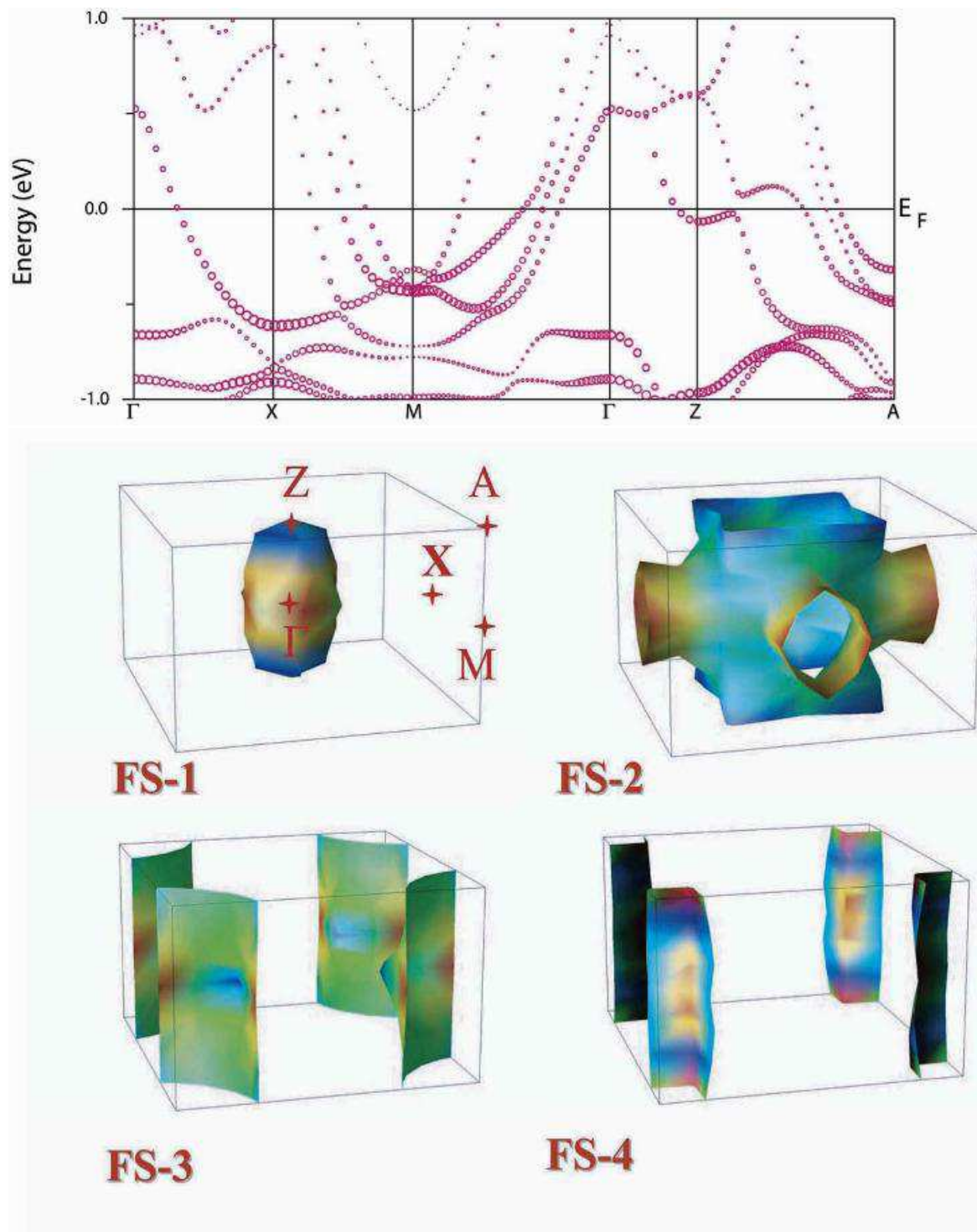


FIG. 9: (Color online) (Top) the band structure; (bottom) Fermi surface of  $\text{PuCoGa}_5$  for  $U = 4$  eV obtained from LDA+ED calculations.

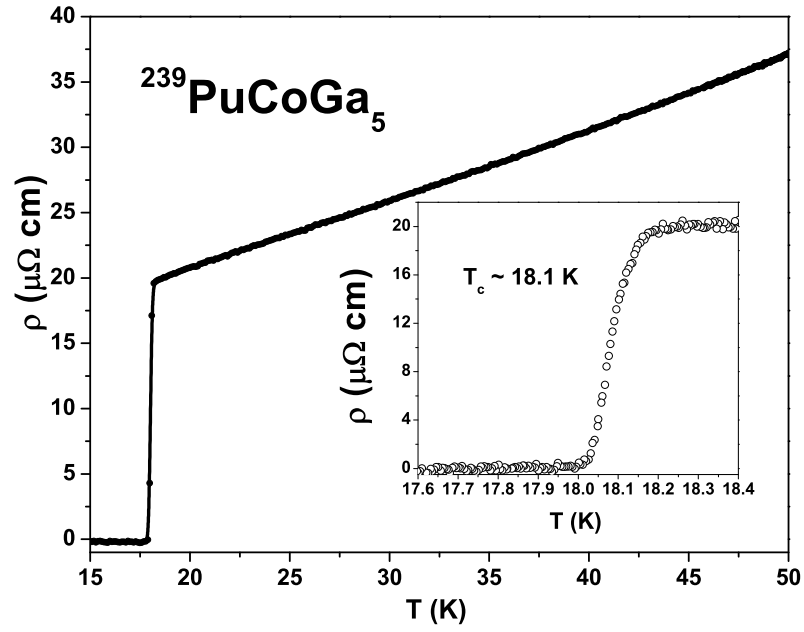


FIG. 10: Temperature dependence of the electrical resistivity of a  $^{239}\text{PuCoGa}_5$  single crystal after thermal annealing of the self-radiation damage.

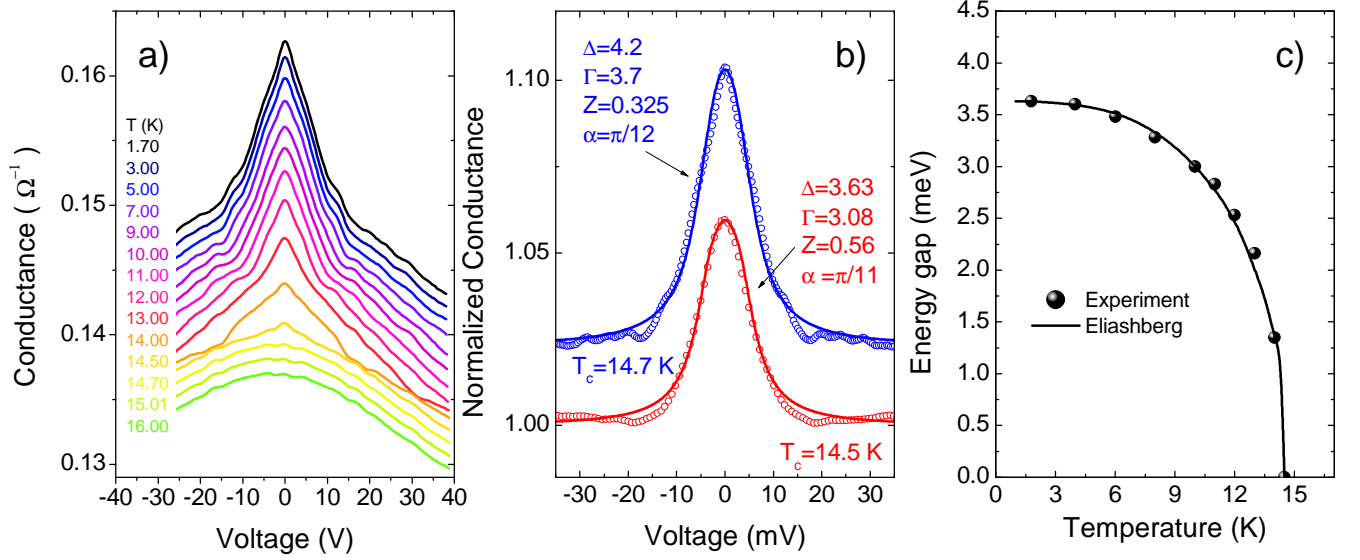


FIG. 11: (a) Temperature dependence of the conductance curves of a contact with  $R_N = 6.9\Omega$  on a  $^{242}\text{PuCoGa}_5$  crystal with reduced  $T_c = 14.5$  K. The curves are vertically offset for clarity. (b) Two examples of low-temperature normalized conductance curves in two contacts on the same crystals (symbols). Lines represent the best-fit of the spectra within the d-wave 2D-BTK model. The normal-state resistance is  $R_N = 6.9 \Omega$  (top) and  $R_N = 18.8 \Omega$  (bottom). (c) Temperature dependence of the gap extracted from the fit of the conductance curves of the contact with  $R_N = 18.8 \Omega$  (symbols). The solid line is the corresponding  $\Delta(T)$  function calculated within the Eliashberg theory by assuming  $\Omega_0 = 6.5$  meV and a coupling constant  $\lambda = 2.37$ .